8-9-2014

ULTRATHIN GRAPHENE OXIDE MEMBRANES/COATINGS FOR SEPARATIONS

Hang Li
University of South Carolina - Columbia

ULTRATHIN GRAPHENE OXIDE MEMBRANES/COATINGS FOR SEPARATIONS

by

Hang Li

Bachelor of Engineering
Dalian University of Technology, 2009

Submitted in Partial Fulfillment of the Requirements

For the Degree of Master of Science in

Chemical Engineering

College of Engineering and Computing

University of South Carolina

2014

Accepted by:

Miao Yu, Director of Thesis

John R. Regalbuto, Reader

James A. Ritter, Reader

John W. Weidner, Reader

Lacy Ford, Vice Provost and Dean of Graduate Studies

DEDICATION

This dissertation work is dedicated to my wife, my parents and parents-in-law,

Philippians 4:7 And the peace of God, which transcends all understanding, will guard your hearts and your minds in Christ Jesus.

ACKNOWLEDGEMENTS

I would like to give my greatest acknowledgement to my advisor, Dr. Miao Yu, for his novel ideas and kind guidance throughout my research projects. Both my experimental skills and theoretical knowledge have been significantly enriched during our daily discussion and interaction. Sincere thanks also go to my MS committee members, Drs. John R. Regalbuto and James A. Ritter, for their precious advices.

I also want to thank all of my friends in USC, who not only offered me academic assistance during my research and study, but also helped me in my personal life. We had a lot of fun together in the past years, and it will become the one of the most valuable memories in my overseas experience.

Dr. Chuck C.Y. Kwok and Mrs. Shirley Kwok, thank you for bringing the evangelism from Lord Jesus Christ to me. My life is fulfilled and becomes fruitful. Dearest brothers and sisters in Chinese Christian Church of Columbia and USC Student Fellowship, thank you for being by my side when I was weak and frustrated.

To my cat Bheem, thank you for making my life full of joyfulness. May you rest in peace.

Last but not least, I am truthfully grateful to my wife, Ying, my parents and parents-in-law, for their love, caring, support and understanding. You always stood by me and encouraged me during these years. I feel really happy to have you as a family.

ABSTRACT

Graphene oxide (GO) was utilized as a novel material for making ultrathin membranes for gas separation and for making functional coatings for nano-/ultra-filtration in oil/water separation. Fundamental separation mechanisms by ultrathin GO membranes/coatings and potential applications were explored. This work can be divided into three parts. In the first part, ultrathin GO membranes supported on flat and smooth anodic aluminum oxide (AAO) substrates, with thickness down to 1.8 nm, were prepared by a facile vacuum filtration method. The as-prepared GO membranes were then studied for single-gas permeation and hydrogen mixture separation. It was revealed that the separation mechanism for the ultrathin GO membranes followed the molecular sieving. Ultrathin GO membranes represent a new type of membranes that may realize high throughput molecular-sieving separation at low energy cost.

In the second part of this work, GO was used as a coating material to modify macroporous polyamide (PA) supports, by a similar vacuum filtration approach. The supported GO membranes showed superoleophobicity and low oil-adhesion underwater. This could be ascribed to the hierarchically rough membrane surface and excellent water "locking" property of GO. The hierarchical roughness was introduced by the combination of the intrinsic micro-scaled roughness of the PA support with the nano-scaled corrugation of GO flakes. Oil/water separation results showed that by optimizing GO coating thickness, antifouling property and 100% pure water flux recovery were achieved.

As an extension of the second section, the third section of the thesis work was focused on tuning oleophobicity of GO coatings under water by gradually modifying the chemistry and structure of GO flakes using ultraviolet (UV) irradiation. The underwater oleophobicity of GO coatings was tuned gradually, simply by controlling the UV treatment time. Oxidative UV etching was shown to generate more and larger structural defects on GO flakes, which increased the nano-scaled roughness on GO flakes. In addition, more hydrophilic oxygen-containing groups, such as carboxyl, carbonyl, hydroxyl and epoxy, introduced by UV irradiation, improved the ability of GO to attract and "lock" water molecules at the coating surface, which effectively lowers oil adhesion. The GO flakes with different UV treatment time were fabricated into GO membranes on PA supports. A series of oil/water separations were conducted for these GO membranes, and membrane recovery capability was greatly improved with the optimized UV etching time.

TABLE OF CONTENTS

LIST OF FIGURES

LIST OF ABBREVIATIONS

AAO ..... Anodic Aluminum Oxide

AFM ..... Atomic Force Microscopy

CA ..... Contact Angle

CN ..... Cellulous Nitrate

FESEM ..... Field Emission Scanning Electron Microscopy

FID..... Flame Ionization Detector

GC ..... Gas Chromatography

GO ..... Graphene Oxide

HRTEM ..... High Resolution Transmission Electron Microscopy

HD ..... Hexadecane

PA..... Polyamide

rGO..... Reduced Graphene Oxide

TCD ..... Thermal Conductivity Detector

TOC ..... Total Organic Carbon

UV ..... Ultraviolet

UV-vis ..... Ultraviolet-Visible Spectroscopy

XPS..... X-ray Photoelectron Spectroscopy

XRD..... X-ray Diffraction

CHAPTER 1: INTRODUCTION AND LITERATURE REVIEW

1.1 Membrane Separation Technology

A membrane is a selective physical barrier that allows certain constituents to permeate through, while retaining other constituents. The influent of a membrane is called the feed, and the flow that passes through the membrane is known as the permeate. The retained is the retentate or concentrate. The mass transport across the membrane is ascribed to the driving force provided by the chemical potential difference between the feed and the permeate[1, 2]. In most situations, the flux is proportional to the driving force, as described by a simple equation[1]:

$$J_i = -A_i \frac{dX_i}{dx}$$

Where Ji is the flux of component i, A_i the proportionality coefficient of component i, and dX_i/dx chemical potential gradient of component i.

The performance of a membrane is typically defined by two parameters, flux and selectivity. For economic separations using membranes, both flux and selectivity need to be considered simultaneously. Flux is the rate at which the permeate passes through a membrane. Higher flux represents higher productivity. Selectivity corresponds to the capability of a membrane to separate a component from a mixture. A selective separation may result from preferential adsorption, diffusion difference, or both.

According to physical and chemical properties, membranes can generally be classified as inorganic and organic membranes, porous and nonporous (dense) membranes, or symmetrical and asymmetrical membranes. However, these classifications are not very strict, since some membranes might belong to more than one category. Carbon[3], silica[4], zeolites[5] and metal[6, 7] membranes are inorganic, while polymeric[8] membranes are organic. Inorganic and polymeric membranes can be either porous or nonporous. For example, carbon, silica, zeolites and some polymeric membranes are porous, while metal and ion exchange membranes[2, 9, 10] are dense. Most microporous membranes and dense membranes are symmetrical membranes, since they have both compositional and structural uniformity across the membrane. Thin film composite membranes[11] are asymmetrical because they are either physically or chemically heterogeneous; a back porous substrate is usually used to support the top thin layer.

The invention of asymmetric polymeric membranes in flat sheet and hollow fiber forms represents a big breakthrough in the membrane separation history. They can be fabricated at high packing density and with low cost for large scale applications[12, 13]. However, certain shortcomings of polymeric membranes severely limit their wide industrial applications, including swelling in organic solvent, compressibility at high pressures, and instability at high temperatures and under harsh chemical conditions. Inorganic membranes may overcome these limitations, but their applications in gas separations are limited. This is because of the great challenge of reproducibly preparing high quality, defect-free inorganic membranes with thin thickness. For example, in gas separations, carbon membranes usually have high selectivity, but flux is low because they are too thick, although carbon nanotube membranes show high permeate flux[14-16]. Zeolite

membranes may possess both high flux and selectivity, but synthesis of defect-free zeolite membranes reproducibly and at low cost is extremely difficult[17, 18]. Graphene-based material, such as graphene and graphene oxide (GO), have been considered as the perfect membrane material, because they are only atomically thick and thus may be made into membranes that minimize transport resistance and maximize permeate flux[19]. Moreover, they are chemically and thermally stable[20, 21], and mechanically strong[22]. Ease of conformation to the substrate and facile fabrication into membranes, also make them very promising candidate for preparing high quality membranes for separations.

1.2 Next Generation Membrane Material: Graphene-based material

Graphene is a two-dimensional (2D) sheet composed of sp^2-hybridized carbon atoms[23, 24]. In 2004, Geim and Novoselov firstly produced graphene sheets by mechanically exfoliating bulk graphite using Scotch tape[25]. Other than this "Scotch tape" or peel-off approach, graphene can also be prepared by chemical vapor deposition (CVD)[26-29], liquid phase exfoliation of graphite[30], and thermal exfoliation of graphite[31, 32].

Graphite oxide is a compound of carbon, oxygen, and hydrogen (ratio of C and O: 2.1~2.9)[33]. It has been prepared by Brodie[34], Staudenmaier[35], and Hummers methods[33] or modified Hummers methods[36-39]. All these methods involve oxidation of graphite in the presence of strong acids and oxidants. The ratio of carbon and oxygen in graphite oxide is variable, depending on the method, the reaction conditions and the precursor graphite being used[40]. Graphene oxide (GO) is a single layer of graphite oxide. Graphene oxide surface is amphiphilic in air[41, 42]. However, it has been shown that only water molecules can intercalate into the inter-layer space between two individual GO sheets , while other molecules cannot due to the sieving effect[43]. The interlayer spacing of graphite, or the

distance between two individual graphene sheets, is 0.34 nm[44]. This value is higher for GO sheets, due to the introduced oxygen containing groups from the oxidative preparation procedure[31, 45-47]. This distance for GO can further increases reversibly from 0.6 to 1.2 nm as the relative humidity increases[48]. Notably, graphite oxide can be completely exfoliated to produce aqueous colloidal dispersions of GO sheets by simple ultrasonication[49]. Several polar solvents, such as ethylene glycol, Dimethylformamide, *N*-Methylpyrrolidone and Tetrahydrofuran, can also disperse graphite oxide at about 0.5 mg/ml[50]. GO sheets, after chemical modification by organic molecules, can also be dispersed homogeneously in other organic solvents[51].

GO can be appropriately reduced to generate reduced graphene oxide (rGO), which has similar chemical and physical properties as graphene. Currently, the mostly used reducing methods include chemical (using reducing agents like hydrazine[52-54], dimethylhydrazine[55], hydroquinone[56] and $NaBH_4$[57, 58]), and thermal reductions[31, 59, 60]. The reduction of GO dispersion in aqueous media results in agglomerated rGO sheets[52]. Elemental analysis of the rGO measured by combustion revealed the existence of a significant amount of oxygen, suggesting that the rGO is not the same as pristine graphene. The atomic ratio of C to O is approximately 10:1. Thermal treatment of graphite oxide is another route to obtain reduced sheets. Rapid heating (>2000 ^{o}C/min) up to 1050 ^{o}C exfoliates as well as reduces graphite oxide. The atomic ratio of C:O after reduction is 10.3, similar to that of hydrazine-reduced GO. The thermally reduced GO sheets can be dispersed in several organic solvents at 0.1 mg/ml.

Recently, porous graphene-based material draws a lot of attention. This material can be described as a graphene or GO sheet with "missing" carbon atoms, leaving

structural defects (holes or pores or vacancies) in the planar structure[61]. Several methods have been proved to be effective to generate structural defects on graphene or GO sheets. Fischbein et al.[62] demonstrated the generation of defects by exposing suspended graphene sheets to a focused electron beam from a transmission electron microscope (TEM) with controlled exposure time. Fox et al.[63] used a low-energy focused electron beam from a scanning electron microscope (SEM) to treat graphene sheets under N_2 atmosphere. They found that the etching occurred when the electron was focused in the presence of nitrogen gas. As a consequence, defects with diameters around 10 nm were successfully created. Koinuma et al.[64] etched GO by UV irradiation in O_2 atmosphere. The GO in this study was prepared by the Hummers method, and then coated on mica. A mercury lamp was applied to provide UV source for the irradiation of GO samples. Koening, et al.[65] reported a similar UV-induced oxidative etching to generate defects on pristine graphene. Other methods, such as plasma etching[66, 67], steam etching[68], and femtosecond laser irradiation[69, 70], etc., have also be demonstrated for defect formation.

1.3 Graphene-Based Membranes for Separations

Graphene, GO and rGO have been fabricated into membranes and shown promising performance in both gas and liquid separations due to their unique "size sieving" effect. Both nano-scaled interlayer spacing between two individual flakes and selective structural defects on the flakes have been claimed to be responsible for the observed separation performance.

1.3.1 For Gas Separations

Nair et al.[43] prepared free-standing GO membranes by spray- or spin-coating of GO dispersion on porous substrates and subsequent transfer to a copper foil with an open hole. They found that sub-micrometer thick GO membranes were completely impermeable to organic vapors and He gas, but allowed unimpeded permeation of water; the proposed water permeation pathway was interlayer spacing between GO flakes. To elucidate the underlying mechanism, the authors reduced a GO membrane by annealing at 250 ^{o}C in a hydrogen-argon mixed atmosphere. It exhibited 100 times less water flux, which was attributed to the narrowed interlayer distance from 1 to 0.4 nm (measured by X-ray diffraction (XRD)). Although He gas cannot permeate through dry GO membranes, , it permeated through GO membranes with the existence of saturated water vapor. XRD results showed that when exposed to water vapor, water molecules can intercalate into the interlayer spacing due to the strong affinity between the oxygen groups and water and thus swell these capillaries; expanded interlayer spacing, therefore, allows He to permeate through. These capillaries also allow low-friction flow of water molecules, while blocking organic molecules. GO membranes, therefore, may have great potential of selective removal of water from organics. This work, for the first time, suggests GO membranes may separate different molecules through interlayer spacing between GO sheets. However, in this preliminary study, very thick GO membranes were prepared and studied for transport of molecules. The major advantage of using graphene-based material for preparing membranes, atomic thickness, therefore, was not realized.

Koenig et al.[65] investigated permeation of different gas molecules through individual porous graphene flakes. Graphene flakes, mechanically exfoliated from

graphite, were suspended over micrometer-sized wells etched into silicon oxide wafer. They used ultraviolet-induced oxidative etching to controllably introduce defects into the pristine graphene flakes. A pressurized blister test and mechanical resonance were used to measure the transport of a range of gases (H_2, CO_2, Ar, N_2, CH_4 and SF_6) through the defects, and a molecular sieving behavior was found. This proof-of-concept work demonstrates great potential of utilizing porous graphene as a promising membrane material for gas separation by molecular sieving. However, only graphene flakes, instead of membranes, were fabricated and tested in this study. Also, investigation of mixture gas separation wasn't performed.

In 2013, our group and another group firstly prepared ultrathin, graphene-based membranes and demonstrated their gas separation performance. Our group[19] fabricated ultrathin GO membrane with thickness approaching 1.8 nm by a facile vacuum filtration process on anodic aluminum oxide (AAO). Single gas permeation was first tested for He, H_2, CO_2, O_2, N_2, CO, and CH_4 molecules through an 18-nm GO membrane, and H_2 permeance was found to be nearly 300 times faster than CO_2. Afterwards, mixture gas separation was conducted and the selectivities were as high as 3400 and 900 for H_2/CO_2 and H_2/N_2 mixtures, respectively. Moreover, we noticed that the H_2 and He permeances decreased exponentially as the membrane thickness increased from 1.8 to 180 nm, which could be due to the particular molecular transport pathway through the selective structural defects on the GO flakes. This conclusion was further strengthened by gas permeation through 18-nm rGO membranes (reduced d-spacing). Similar behavior as 18-nm GO membranes was observed, indicating that interlayer spacing is not the major transport pathway. This study suggests that ultrathin GO membranes may have wide applications

in pre-combustion CO_2 capture and H_2 recovery for ammonia production. This work is part of this thesis, as discussed in detail in Chapter 2.

Kim et al.[71] from Hanyang University in South Korea also investigated the gas permeation through ultrathin GO membranes. They found GO membranes in the dry state were not permeable to gasses. However, water molecules intercalated in the GO interlayer spacing, which generated nanometer-sized pores and channels. These opened channels allowed permeation of gas molecules. The authors found that the gases can permeate through thick GO membranes when sufficient pressure was applied in order to overcome the energy barrier for pore entry and diffusion. Also, the gas permeability could be tuned by changing the GO flake size. They also demonstrated that a high CO_2/N_2 selectivity could be achieved when they varied the humidity levels in the feed streams of the GO membranes. Therefore, GO membranes may potentially be used to capture carbon dioxide from flue gas.

Celebi et al.[72] reported a reliable method for creating 2D graphene membranes using CVD optimized to grow graphene with minimal defects and cracks to form graphene layers thinner than 1 nm. Using a focused ion beam (FIB), they drilled nanopores in double layers of graphene to produce porous membranes with aperture diameters between less than 10 and 1000 nm. They found that the graphene membranes had water permeance five to seven times higher than conventional filtration membranes and water vapor flux was several hundred times higher than today's most advanced breathable textiles. This finding may lead to the development of highly breathable filters that are waterproof and effective to separate dangerous gases from air.

1.3.2 For Water Purification

Hu and Mi[73] reported a novel procedure to fabricate ultrathin GO membranes that allow water to flow through the nanochannels between GO layers while blocking unwanted large solutes by size sieving and charge effects. The GO membranes were made via layer-by-layer deposition using GO dispersion. GO flakes were cross-linked by 1,3,5-benzenetricarbonyl trichloride on a polydopamine-coated polysulfone support. They found that the cross-linking was essential to provide the GO membranes with stability in water, as well as tune the charges, functionality, and spacing of the GO nanosheets. GO membranes were used to test the salt and dye rejections. Although the GO membranes exhibited a relatively low rejection (6-46%) of monovalent and divalent salts, it showed a moderate rejection (46-66%) for Methylene blue and a high rejection (93-95%) for Rhodamine-WT. Water flux of the GO membranes was 4 to 10 times higher than that of commercially available nanofiltration membranes.

In a separate study, Qiu et al.[74] reported an approach to create corrugation on rGO flakes by hydrothermal treatment of the rGO dispersions. The researchers revealed that the amplitude of GO corrugation can be simply controlled by hydrothermal treatment temperature, and the corrugation could form nanochannels in the rGO membranes. This statement was supported by two types of filtration experiments. In the first one, colloids of Au and Pt nanoparticles with average diameters of ~13 and ~3 nm, respectively, were utilized for a series of filtration tests. As a result, the 90-rGO (rGO hydrothermally treated at 90 ^{o}C) membrane showed no permeation for both Au and Pt, indicating a channel size smaller than 3 nm. 100- and 120-rGO membranes allowed only Pt to pass through, suggesting the existence of nanochannels with a size of 3 to 13 nm. 150-rGO

couldn't reject either two particles. In the second filtration test, direct yellow (DY) solution was employed in filtration tests, and again the rejection of DY decreased as the hydrothermal temperature increased,.

Han et al.[75] developed a reduction route to convert GO to rGO. GO dispersion and NaOH were firstly mixed together with stirring under nitrogen flow and then heated to reflux until uniform rGO dispersion resulted. A vacuum filtration was applied to deposit ultrathin rGO membranes, with thickness from 22 to 53 nm. The prepared rGO membranes showed layered structure. The performance of the rGO membranes for water treatment was evaluated on a dead end filtration device, and the pure water flux reached up to 21.8 L $m^{-2}h^{-1}bar^{-1}$. These membrane also exhibited high rejection (>99%) for organic dyes and moderate rejection (20 to 60%) for salts. The rejection mechanism of the negatively charged membranes, as the authors claimed, was a combination of physical sieving and electrostatic interaction.

Joshi et al.[76, 77] prepared GO membranes by vacuum filtration of GO dispersion. These GO membranes showed vacuum-tight in the dry state, but if immersed in water, they acted as molecular sieves, blocking all solutes with hydrated radii larger than 0.45 nm. Smaller ions permeated through the GO membranes at rates thousands of times faster than what is expected for simple diffusion. The authors believed that this behavior is caused by a network of nanocapillaries that open up in the hydrated state and accept only species that fit in. The ultrafast permeation is attributed to a capillary-like high pressure on ions inside GO capillaries.

1.3.3 For Water/Organic Solvent Pervaporation

Yeh et al.[78] fabricated GO membranes with thickness from 90 to 300 nm for ethanol dehydration, by either vacuum filtration or spinning coating onto a thin-film nanofibrous composite (TFNC). Pervaporation results showed that a 93 nm thick GO membrane had a permeate flux of 2.2 kg m^{-2} h^{-1} and a separation factor of 308 for a feed of 80 wt% ethanol in water at 70 ^{o}C. The authors inferred the water transport pathway was through the interlayer spacing.

Tang et al.[79] reported free-standing GO membranes assembled by a pressurized ultrafiltration method. Experimental results suggested that the interlayer spacing was determined by both packing density of GO nanosheets and water content in the feed solution. The packing density was sensitively affected by the ultrafiltration pressure applied during membrane formation. By tuning the ultrafiltration pressure, a high separation performance with water permeability of 13800 Barrer (1 Barrer = 3.348×10^{-19} kmol m m^{-2} s^{-1} Pa^{-1}) and water/ethanol selectivity of 227 was achieved for dehydration of an 85 wt% ethanol aqueous solution at 24 ^{o}C.

Huang et al.[80] demonstrated a GO membrane prepared by vacuum filtration onto a ceramic hollow fiber. This GO membrane exhibited excellent water permeation of dimethyl carbonate/water mixtures through a pervaporation process. At 25 ^{o}C, for a feed with 2.6 wt% water, the permeate contained 95.2 wt% water and had a flux of 1702 g m^{-2} h^{-1}.

1.4 Thesis Scope

The main objective of this thesis is to study the fundamental material properties of GO and utilize their chemical and structural properties to prepare nanostructured GO membranes for separation applications. Chapter 2 introduces the preparation and characterization of ultrathin GO membranes, and discusses gas permeation mechanisms and separation performance for H_2 mixtures. Chapter 3 demonstrates a novel design of GO membrane structure that shows underwater superoleophobicity and antifouling performance in oil/water emulsion separation. Chapter 4 discusses a facile method, UV oxidative etching, for fine tuning the GO chemistry and flake morphology, and then demonstrates its potential of improving the surface chemistry and roughness of GO flakes for oily wastewater treatment. Chapter 5 gives conclusions for this thesis.

1.5 References

1. R. W. Baker, Membrane Technology and Applications, Wiley, Weinheim, 2004.
2. F. G. Donnan, Journal of Membrane Science, 1995, 100, 45-55.
3. M. B. Shiflett and H. C. Foley, Science, 1999, 285, 1902-1905.
4. R. M. de Vos and H. Verweij, Science, 1998, 279, 1710-1711.
5. Z. Lai, G. Bonilla, I. Diaz, J. G. Nery, K. Sujaoti, M. A. Amat, E. Kokkoli, O. Terasaki, R. W. Thompson and M. Tsapatsis, Science, 2003, 300, 456-460.
6. A. L. Athayde, R. W. Baker and P. Nguyen, Journal of Membrane Science, 1994, 94, 299-311.
7. R. B. McBride and D. L. McKinley, Chem. Eng. Prog., 1965, 61, 81-&.
8. H. B. Park, C. H. Jung, Y. M. Lee, A. J. Hill, S. J. Pas, S. T. Mudie, E. Van Wagner, B. D. Freeman and D. J. Cookson, Science, 2007, 318, 254-258.
9. T. R. E. Kressman, Nature, 1950, 165, 568-568.
10. W. Juda and W. A. McRae, Journal of the American Chemical Society, 1950, 72, 1044-1044.
11. Materials Science of Synthetic Membranes, American Chemical Society, 1985.
12. W. W. Ho and K. K. Sirkar, Membrane handbook, Springer, 1992.
13. M. Freemantle, Chemical & Engineering News Archive, 2005, 83, 49-57.
14. M. Majumder, N. Chopra, R. Andrews and B. J. Hinds, Nature, 2005, 438, 44-44.
15. B. J. Hinds, N. Chopra, T. Rantell, R. Andrews, V. Gavalas and L. G. Bachas, Science, 2004, 303, 62-65.
16. J. K. Holt, H. G. Park, Y. Wang, M. Stadermann, A. B. Artyukhin, C. P. Grigoropoulos, A. Noy and O. Bakajin, Science, 2006, 312, 1034-1037.

17. N. W. Ockwig and T. M. Nenoff, Chemical Reviews, 2007, 107, 4078-4110.

18. T. C. Bowen, H. Kalipcilar, J. L. Falconer and R. D. Noble, Journal of Membrane Science, 2003, 215, 235-247.

19. H. Li, Z. N. Song, X. J. Zhang, Y. Huang, S. G. Li, Y. T. Mao, H. J. Ploehn, Y. Bao and M. Yu, Science, 2013, 342, 95-98.

20. D. A. Dikin, S. Stankovich, E. J. Zimney, R. D. Piner, G. H. B. Dommett, G. Evmenenko, S. T. Nguyen and R. S. Ruoff, Nature, 2007, 448, 457-460.

21. S. Chen, L. Brown, M. Levendorf, W. Cai, S.-Y. Ju, J. Edgeworth, X. Li, C. W. Magnuson, A. Velamakanni, R. D. Piner, J. Kang, J. Park and R. S. Ruoff, ACS Nano, 5, 1321-1327.

22. C. Lee, X. D. Wei, J. W. Kysar and J. Hone, Science, 2008, 321, 385-388.

23. A. K. Geim and K. S. Novoselov, Nature materials, 2007, 6, 183-191.

24. S. Park and R. S. Ruoff, Nat Nano, 2009, 4, 217-224.

25. K. S. Novoselov, A. K. Geim, S. V. Morozov, D. Jiang, Y. Zhang, S. V. Dubonos, I. V. Grigorieva and A. A. Firsov, Science, 2004, 306, 666-669.

26. M. Eizenberg and J. M. Blakely, Surface Science, 1979, 82, 228-236.

27. K. S. Kim, Y. Zhao, H. Jang, S. Y. Lee, J. M. Kim, K. S. Kim, J.-H. Ahn, P. Kim, J.-Y. Choi and B. H. Hong, Nature, 2009, 457, 706-710.

28. P. W. Sutter, J.-I. Flege and E. A. Sutter, Nat Mater, 2008, 7, 406-411.

29. A. Reina, X. Jia, J. Ho, D. Nezich, H. Son, V. Bulovic, M. S. Dresselhaus and J. Kong, Nano Letters, 2008, 9, 30-35.

30. Y. Hernandez, V. Nicolosi, M. Lotya, F. M. Blighe, Z. Sun, S. De, I. T. McGovern, B. Holland, M. Byrne, Y. K. Gun'Ko, J. J. Boland, P. Niraj, G. Duesberg, S.

Krishnamurthy, R. Goodhue, J. Hutchison, V. Scardaci, A. C. Ferrari and J. N. Coleman, Nat Nano, 2008, 3, 563-568.

31. M. J. McAllister, J.-L. Li, D. H. Adamson, H. C. Schniepp, A. A. Abdala, J. Liu, M. Herrera-Alonso, D. L. Milius, R. Car, R. K. Prud'homme and I. A. Aksay, Chemistry of Materials, 2007, 19, 4396-4404.

32. D. D. L. Chung, Journal of Materials Science, 1987, 22, 4190-4198.

33. W. S. Hummers and R. E. Offeman, Journal of the American Chemical Society, 1958, 80, 1339-1339.

34. B. C. Brodie, Philosophical Transactions of the Royal Society of London, 1859, 149, 249-259.

35. L. Staudenmaier, Berichte der deutschen chemischen Gesellschaft, 1898, 31, 1481-1487.

36. N. I. Kovtyukhova, P. J. Ollivier, B. R. Martin, T. E. Mallouk, S. A. Chizhik, E. V. Buzaneva and A. D. Gorchinskiy, Chemistry of Materials, 1999, 11, 771-778.

37. H. A. Becerril, J. Mao, Z. Liu, R. M. Stoltenberg, Z. Bao and Y. Chen, ACS Nano, 2008, 2, 463-470.

38. Z. Liu, Q. Liu, Y. Huang, Y. Ma, S. Yin, X. Zhang, W. Sun and Y. Chen, Advanced Materials, 2008, 20, 3924-3930.

39. D. Li, M. B. Muller, S. Gilje, R. B. Kaner and G. G. Wallace, Nat Nano, 2008, 3, 101-105.

40. D. R. Dreyer, S. Park, C. W. Bielawski and R. S. Ruoff, Chemical Society Reviews, 39, 228-240.

41. N. Withers, Nat Chem.

42. J. Kim, L. J. Cote, F. Kim, W. Yuan, K. R. Shull and J. Huang, Journal of the American Chemical Society, 132, 8180-8186.

43. R. R. Nair, H. A. Wu, P. N. Jayaram, I. V. Grigorieva and A. K. Geim, Science, 2012, 335, 442-444.

44. G. Bacon, Acta Crystallographica, 1951, 4, 558-561.

45. H.-K. Jeong, Y. P. Lee, M. H. Jin, E. S. Kim, J. J. Bae and Y. H. Lee, Chemical Physics Letters, 2009, 470, 255-258.

46. A. Lerf, A. Buchsteiner, J. Pieper, S. Schottl, I. Dekany, T. Szabo and H. Boehm, Journal of Physics and Chemistry of Solids, 2006, 67, 1106-1110.

47. S. Cerveny, F. Barroso-Bujans, A. Alegria and J. Colmenero, The Journal of Physical Chemistry C, 114, 2604-2612.

48. A. Buchsteiner, A. Lerf and J. Pieper, The Journal of Physical Chemistry B, 2006, 110, 22328-22338.

49. S. Stankovich, R. D. Piner, X. Chen, N. Wu, S. T. Nguyen and R. S. Ruoff, Journal of Materials Chemistry, 2006, 16, 155-158.

50. J. Paredes, S. Villar-Rodil, A. Martinez-Alonso and J. Tascon, Langmuir, 2008, 24, 10560-10564.

51. S. Stankovich, R. D. Piner, S. T. Nguyen and R. S. Ruoff, Carbon, 2006, 44, 3342-3347.

52. S. Stankovich, D. A. Dikin, R. D. Piner, K. A. Kohlhaas, A. Kleinhammes, Y. Jia, Y. Wu, S. T. Nguyen and R. S. Ruoff, Carbon, 2007, 45, 1558-1565.

53. J. R. Lomeda, C. D. Doyle, D. V. Kosynkin, W.-F. Hwang and J. M. Tour, Journal of the American Chemical Society, 2008, 130, 16201-16206.

54. V. C. Tung, M. J. Allen, Y. Yang and R. B. Kaner, Nature nanotechnology, 2009, 4, 25-29.

55. S. Stankovich, D. A. Dikin, G. H. Dommett, K. M. Kohlhaas, E. J. Zimney, E. A. Stach, R. D. Piner, S. T. Nguyen and R. S. Ruoff, Nature, 2006, 442, 282-286.

56. G. Wang, J. Yang, J. Park, X. Gou, B. Wang, H. Liu and J. Yao, The Journal of Physical Chemistry C, 2008, 112, 8192-8195.

57. Y. Si and E. T. Samulski, Nano Letters, 2008, 8, 1679-1682.

58. R. Muszynski, B. Seger and P. V. Kamat, The Journal of Physical Chemistry C, 2008, 112, 5263-5266.

59. T. Ramanathan, A. Abdala, S. Stankovich, D. Dikin, M. Herrera-Alonso, R. Piner, D. Adamson, H. Schniepp, X. Chen and R. Ruoff, Nature nanotechnology, 2008, 3, 327-331.

60. H. C. Schniepp, J.-L. Li, M. J. McAllister, H. Sai, M. Herrera-Alonso, D. H. Adamson, R. K. Prud'homme, R. Car, D. A. Saville and I. A. Aksay, The Journal of Physical Chemistry B, 2006, 110, 8535-8539.

61. M. Bieri, M. Treier, J. Cai, K. Ait-Mansour, P. Ruffieux, O. Groning, P. Groning, M. Kastler, R. Rieger, X. Feng, K. Mullen and R. Fasel, Chemical Communications, 2009, 6919-6921.

62. M. D. Fischbein and M. Drndic, Applied Physics Letters, 2008, 93, -.

63. D. Fox, A. O'neill, D. Zhou, M. Boese, J. N. Coleman and H. Z. Zhang, Applied Physics Letters, 98, -.

64. M. Koinuma, C. Ogata, Y. Kamei, K. Hatakeyama, H. Tateishi, Y. Watanabe, T. Taniguchi, K. Gezuhara, S. Hayami, A. Funatsu, M. Sakata, Y. Kuwahara, S. Kurihara and Y. Matsumoto, The Journal of Physical Chemistry C, 116, 19822-19827.

65. S. P. Koenig, L. Wang, J. Pellegrino and J. S. Bunch, Nature nanotechnology, 7, 728-732.

66. Z. Zeng, X. Huang, Z. Yin, H. Li, Y. Chen, H. Li, Q. Zhang, J. Ma, F. Boey and H. Zhang, Advanced Materials, 24, 4138-4142.

67. M. M. Lucchese, F. Stavale, E. H. M. Ferreira, C. Vilani, M. V. O. Moutinho, R. B. Capaz, C. A. Achete and A. Jorio, Carbon, 48, 1592-1597.

68. T. H. Han, Y.-K. Huang, A. T. L. Tan, V. P. Dravid and J. Huang, Journal of the American Chemical Society, 133, 15264-15267.

69. H. O. Jeschke, M. E. Garcia and K. H. Bennemann, Physical Review Letters, 2001, 87, 015003.

70. Y. Miyamoto, H. Zhang and D. Tomanek, Physical Review Letters, 104, 208302.

71. H. W. Kim, H. W. Yoon, S. M. Yoon, B. M. Yoo, B. K. Ahn, Y. H. Cho, H. J. Shin, H. Yang, U. Paik, S. Kwon, J. Y. Choi and H. B. Park, Science, 2013, 342, 91-95.

72. K. Celebi, J. Buchheim, R. M. Wyss, A. Droudian, P. Gasser, I. Shorubalko, J.-I. Kye, C. Lee and H. G. Park, Science, 344, 289-292.

73. M. Hu and B. Mi, Environmental Science & Technology, 47, 3715-3723.

74. L. Qiu, X. Zhang, W. Yang, Y. Wang, G. P. Simon and D. Li, Chemical Communications, 47, 5810-5812.

75. Y. Han, Z. Xu and C. Gao, Advanced Functional Materials, 23, 3693-3700.

76. R. K. Joshi, P. Carbone, F. C. Wang, V. G. Kravets, Y. Su, I. V. Grigorieva, H. A. Wu, A. K. Geim and R. R. Nair, Science, 343, 752-754.

77. B. Mi, Science, 343, 740-742.

78. T.-M. Yeh, Z. Wang, D. Mahajan, B. S. Hsiao and B. Chu, Journal of Materials Chemistry A, 1, 12998-13003.

79. Y. P. Tang, D. R. Paul and T. S. Chung, pp. 199-208.

80. K. Huang, G. Liu, Y. Lou, Z. Dong, J. Shen and W. Jin, Angewandte Chemie International Edition.

CHAPTER 2: ULTRATHIN, MOLECULAR-SIEVING GRAPHENE OXIDE MEMBRANES FOR HIGHLY SELECTIVE HYDROGEN SEPARATION

2.1 Abstract

Ultrathin, molecular-sieving membranes have great potential to realize high flux, high selectivity mixture separation at low energy cost. Current microporous membranes (pore size < 1 nm), however, are usually relatively thick. It is difficult to prepare ultrathin (< 20 nm) microporous membranes without introducing extra defects using current membrane materials and preparation techniques. We report ultrathin graphene oxide (GO) membranes prepared by a facile filtration process with thickness approaching 1.8 nm. These membranes showed mixture separation selectivities as high as 3400 and 900 for H_2/CO_2 and H_2/N_2 mixtures, respectively, through the selective structural defects on GO.

One Sentence Summary: Ultrathin graphene oxide membranes showed much higher separation selectivities for H_2 mixtures than microporous membranes.

2.2 Introduction

Zeolites (*1*) (*2*), silica (*3*), carbon (*4*), and polymers (*5*) have been made into microporous membranes that have shown promising gas mixture separation performance. These membranes separate mixtures based on selective adsorption, diffusion rate

differences, or molecular sieving mechanisms. Current microporous membranes, however, are usually thicker than 20 nanometers in order to minimize undesirable flux contribution through non-selective membrane defects and maintain reasonably high separation selectivity.

Graphene-based materials, such as graphene and graphene oxide (GO), have been considered as promising membrane materials, because they are only one carbon atom thick and thus may form separation membranes that minimize transport resistance and maximize flux. Additionally, they have good stability (*6, 7*) and are mechanically strong (*8*). Graphene-based materials have been made into centimeter-sized, thick (~1 μm) membranes and micrometer-sized, isolated single sheets for pure component permeation studies where they were found to be either impermeable to small gas molecules or not practical for separation applications (*9-12*).

2.3 Experimental Results and Discussion

We used single-layered GO flakes, prepared by the modified Hummer's method (*13*). Ultrathin GO membranes were prepared by vacuum filtration, as described in detail in Figure 2.1. X-ray diffraction (XRD) shows the characteristic peak of GO at 2θ of 11.1° (Figure 2.2 and discussion in (13)). Centrifugation and dilution of GO dispersions were found to be critical for preparing high quality GO membranes (Figure 2.3 and discussion in (13)). Figure 2.4A shows a ca. 9-nm thick GO membrane with a permeation area of ~4 cm^2 on anodic aluminum oxide (AAO) support. GO flakes are about 500 nm in size and single layered, as confirmed by the atomic force microscopy (AFM) image (Figure 2.4B) as well as the height profile of a GO flake (Figure 2.4C). Figures 2.4D and E show the surface of an 18-nm thick GO membrane on AAO. We deposited a relatively thick GO

membrane, approximately 180 nm (Figure 2.4G), to correlate the GO amount with the membrane thickness. GO dispersion for this 180-nm membrane preparation was then diluted 100, 20, and 10 times to obtain the above 1.8-, 9-, and 18-nm thick GO membranes, assuming no GO loss during filtration and constant membrane density. Compared with AAO support (Figure 2.4F)), a very thin GO coating can be clearly seen. X-ray photoelectron spectroscopy (XPS) was used to detect surface elements for these ultrathin GO membranes on AAO (Figures 2.4H and I)). For a 1.8-nm thick membrane, a significant amount of aluminum in AAO can still be seen because the mean free path of excited electrons is longer than the surface GO membrane thickness. However, for thicker membranes (9 and 18 nm), much smaller amounts of underlying aluminum in AAO can be seen because GO thickness is larger than the excited electron mean free path. This is consistent with surface carbon detection by XPS as well (Figure 2.4I). See Supplementary Materials for detailed analysis.

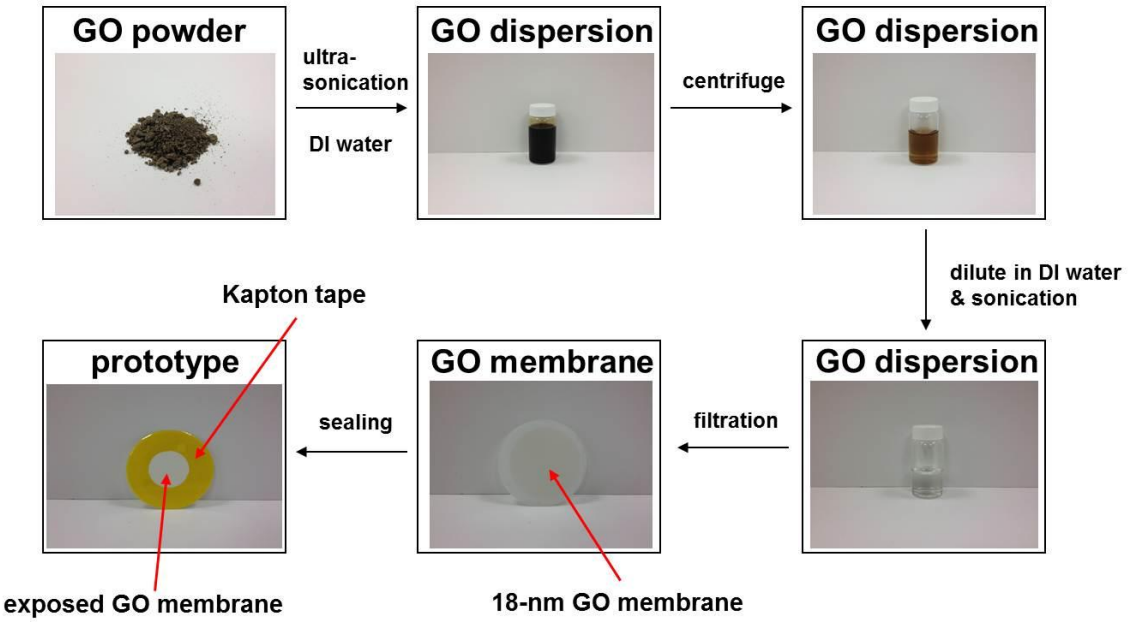

Figure 2. 1 Fabrication process of GO membranes

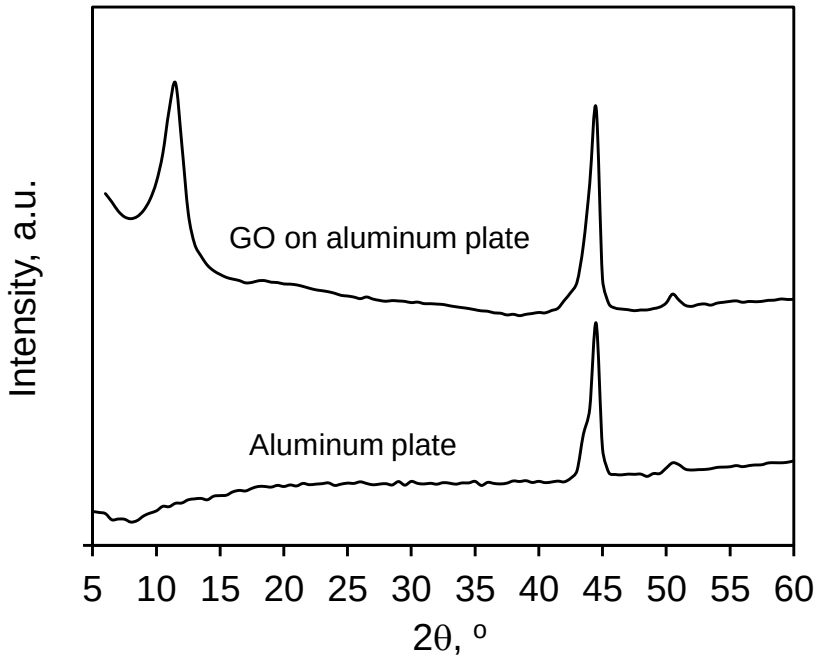

Figure 2. 2 XRD patterns for (A) GO powder on Al plate and (B) blank Al plate

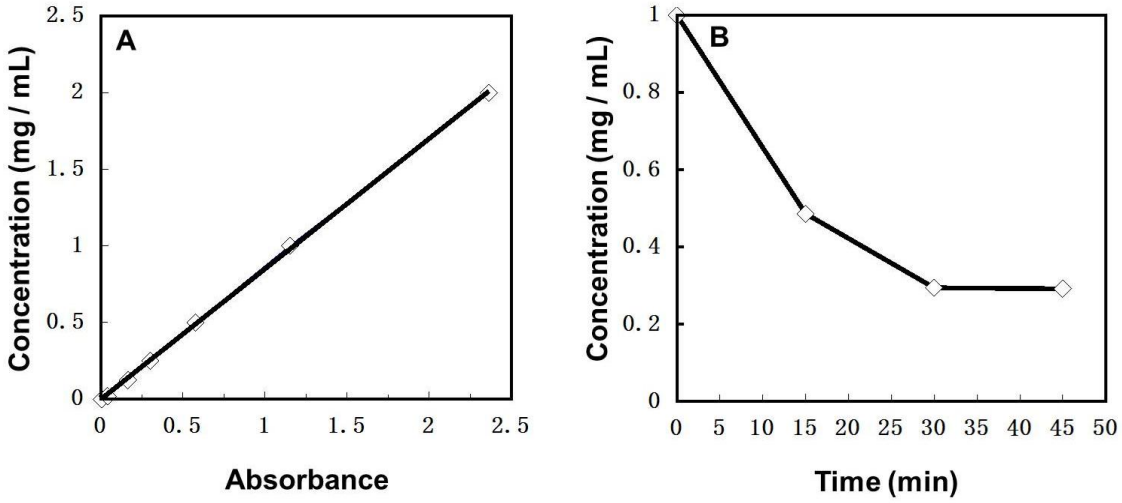

Figure 2. 3 For determination of the GO dispersion concentration after centrifuge, we used UV-vis to measure the absorbance of the prepared standard GO dispersion (0, 0.02, 0.125, 0.25, 0.5, 1 and 2 mg/mL) and found out the concentration of GO dispersion has an excellent linear fit with the UV absorbance, as shown in fig. S1A. Figure S1B shows the dependence of GO concentration on the centrifuge time at 10,000 rpm.

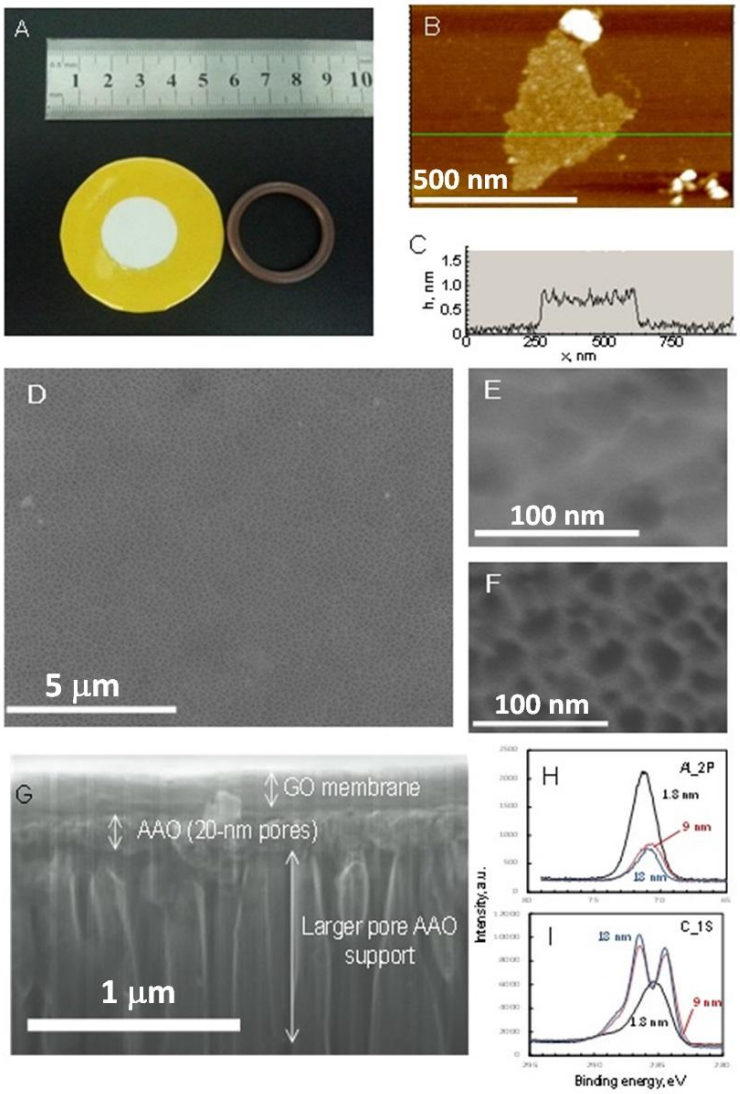

Figure 2. 4 GO membranes supported on porous AAO. (**A**) Digital picture of an ultrathin GO membrane on AAO (ca. 9 nm); middle open white area is the permeation area (~4 cm^2) with supported GO, and yellow Kapton tape is for GO protection and for sealing by O-ring during permeation measurements. (**B**) AFM image of a GO flake on freshly cleaved mica. (**C**) The height profile across the green line in (B). (**D**) Field emission scanning electron microscopy (FE-SEM) image of the surface of a GO membrane (ca. 18-nm thick) on porous AAO. (**E**) FE-SEM image of the GO membrane surface (ca. 18-nm thick) with higher magnification and (**F**) AAO surface without GO membrane. (**G**) FE-SEM image of the cross-sectional view of a thick GO membrane (~180 nm); ultrathin GO membranes (1.8, 9, and 18 nm) were prepared by diluting GO filtration solution for the 180-nm thick membrane in (G) by 100, 20, and 10 times, while maintaining total filtration solution volume constant at 25 ml. (**H**) Al 2P and (**I**) C 1S XPS spectra of ultrathin GO membranes (ca. 1.8, 9, and 18 nm thick) supported on porous AAO. Scale bars in (B), 500 nm; in (D), 5 μm; in (E) and (F), 100 nm; in (G), 1 μm.

We conducted permeation tests with different light gas molecules to probe pore sizes using a glass membrane module (Figure 2.5). Hydrogen (kinetic diameter: 0.289 nm) permeated approximately 300 times faster than CO_2 (0.33 nm) through a ca. 18-nm thick GO membrane at 20 ^oC (Figure 2.6A). Their kinetic diameter differences are only 0.04 nm, suggesting the average size of pores for permeation in the GO membrane may be between 0.289 nm and 0.33 nm. O_2 and N_2 showed similar permeance as CO_2. However, CO and CH_4 had slightly higher permeance, although they are slightly larger. Koenig *et al's* (*12*) also found CH_4 had slightly higher permeance than N_2 through pristine graphene flakes. The reason is still unclear. Figure 2.6B shows H_2 and He permeances for GO membranes with different thickness. Gas permeance is usually inversely proportional to the membrane thickness for conventional membranes (*14*). Surprisingly, we found H_2 and He permeances decrease exponentially as membrane thickness increases from 1.8 to 180 nm for our membranes (Figure 2.6B). We speculate that the major transport pathway for these molecules is selective structural defects on GO flakes, instead of spacing between GO flakes. Reduction has been shown as an effective way to narrow interlayer spacing in GO membranes and thus limit permeation of molecules through spacing *(10)*. We reduced ultrathin GO membranes with thickness from 1.8-20 nm and conducted pressure-driven water permeation. We found water permeance decreased approximately 3 orders of magnitude after reduction; for example, water permeance through a 3-nm GO membranes was 1370 L/(m^2·h·bar), while it was 0.5-1 L/(m^2·h·bar) through reduced GO membrane. This is in agreement with Nair et al.'s finding *(10)* and suggests interlayer spacing has been eliminated or significantly narrowed by reduction. We then measured single-gas permeation through 18-nm reduced GO membranes (Figure 2.7); no obvious

gas permeance change was found, suggesting interlayer spacing is not be the major transport pathway and permeation of molecules is attributed to the selective structural defects on GO flakes. Exponential dependence of gas permeances on membrane thickness (Figure 2.6B) may result from the particular transport pathway of molecules through these selective structural defects in layered GO membranes. Various defects on graphene have been found to be able to separate H_2 from other small molecules (N_2, CH_4 etc.) (*15-17*). The molecular-sieving behavior of H_2 over other molecules may be attributed to the intrinsic defects on GO flakes in our membranes. The Raman spectrum suggests the existence of defects on GO flakes (Figure 2.8 and analysis in (*13*)). Koenig *et al.*(*12*) found H_2/N_2 ideal selectivity for isolated graphene sheets was higher than 10,000 after etching graphene by UV-induced oxidation. We noticed that some of their graphene sheets before etching showed high ideal selectivities for H_2/CH_4 (~100) and H_2/N_2 (~100), indicating intrinsic defects on graphene may also have decent molecular-sieving behavior. Our single-gas permeation results were consistent with their observation. We also extrapolated He permeance for a 1-μm thick GO membrane using an exponential fit in Figure 2.6B and found it is appropriately 10^{-16} mol/(m^2·s·Pa). This explains why the 1-μm thick GO membranes prepared by Nair *et al.* were impermeable to He (*10*). Therefore, for practical separation application of GO membranes, ultrathin thickness is essential in order to have reasonably high gas permeances. Separation of H_2 from other small molecules has important applications, such as pre-combustion CO_2 capture and H_2 recovery for ammonia production (*18-21*).

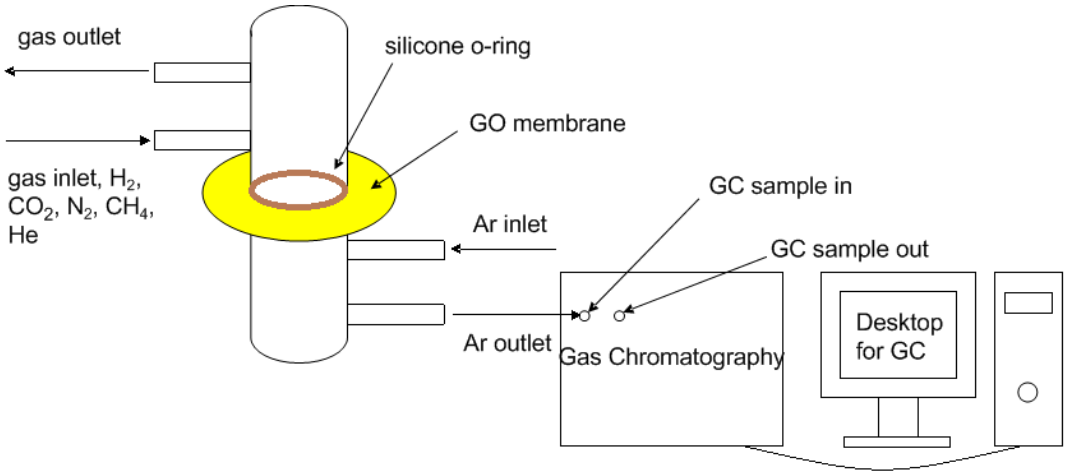

Figure 2. 5 Schematic drawing of gas permeation measurement system

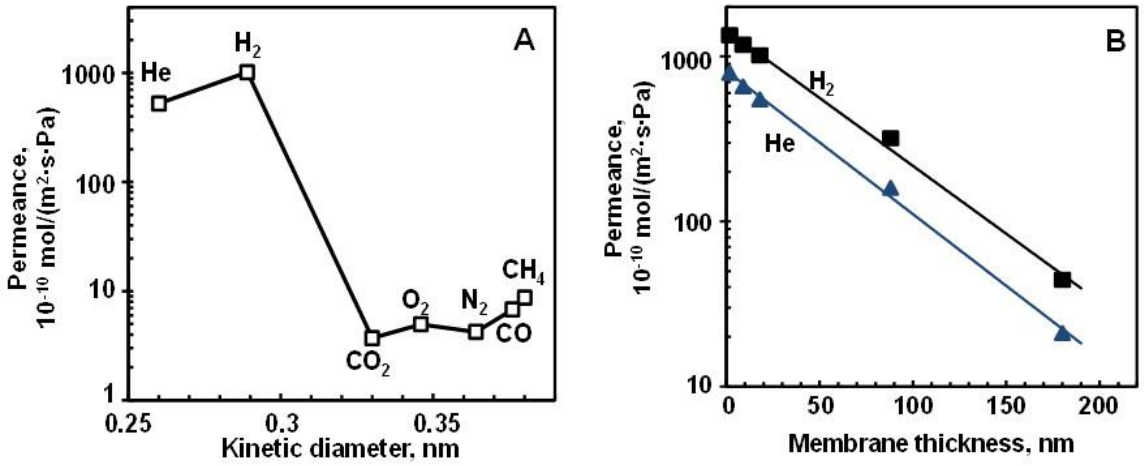

Figure 2. 6 Single-gas permeation through GO membranes supported on porous AAO at 20 ^{o}C. (A) Permeances of seven molecules through a ca. 18-nm thick GO membrane. (**B**) Permeances of H_2 and He through GO membranes with different thicknesses. Lines in (B) are exponential fits.

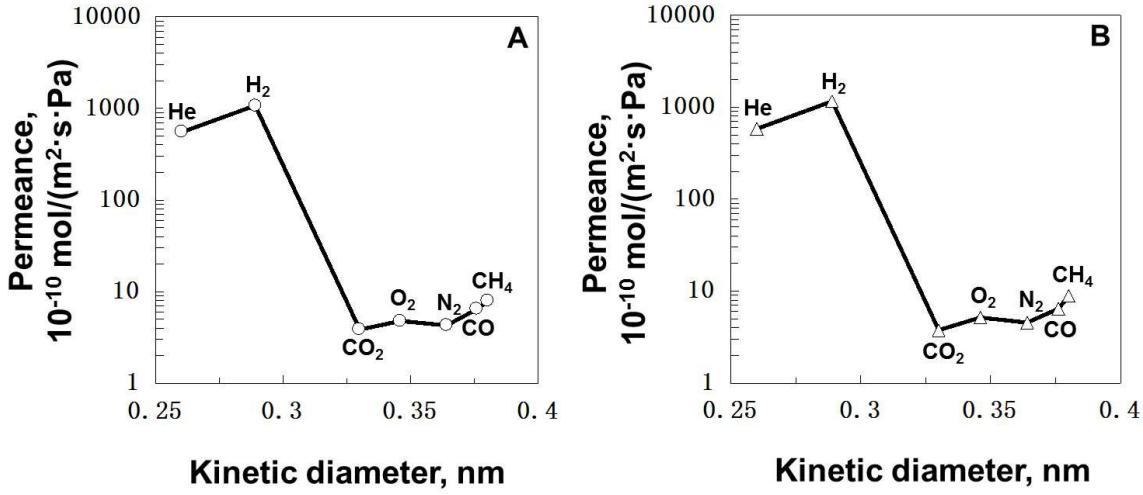

Figure 2. 7 Permeances of seven molecules at 20 ℃ through a ca. 18-nm thick (A) 5% H_2 in Ar reduced GO membrane, and (B) vacuum reduced GO membrane. Both membranes were supported on porous AAO.

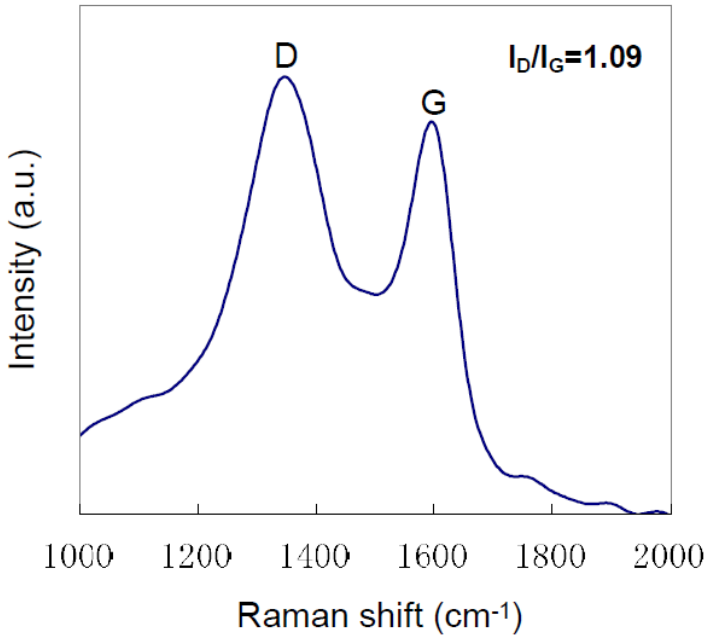

Figure 2. 8 Raman spectrum of the GO powder. The I_D/I_G ratio is 1.09 as shown in the figure.

Separation selectivity and permeance are two important parameters to evaluate membrane separation performance. Before evaluating separation performance of ultrathin GO membranes, a control experiment was first conducted for an AAO support; we found

that the gas permeances were high (> 10^{-6} mol/(m^2·s·Pa)) and selectivities of H_2 over CO_2 and N_2 were low (< 5), as expected for Knudsen diffusion through 20-nm pores. Figure 2.9 shows separation results of 50/50 H_2/CO_2 and 50/50 H_2/N_2 mixtures for 1.8-, 9-, and 18-nm thick GO membranes. All the GO membranes showed high H_2/CO_2 selectivity (> 2,000) at 20 ^oC, with a value of 3,400 for the 9-nm thick membrane. This is unusual, because microporous membranes reported in the literature showed low H_2/CO_2 selectivity (<10) or were selective to CO_2 over H_2 at < 100 ^oC due to strong CO_2 adsorption and blocking of H_2 permeation (*22-24*). Adsorption isotherms on GO powder at 20 ^oC showed much stronger CO_2 adsorption than H_2 (Figure 2.10). These results suggest a molecular-sieving separation of H_2 from CO_2, since strongly adsorbed CO_2 on GO flakes has negligible effects on H_2 permeation, meaning CO_2 can't fit into most of the structural defects on GO that only allow H_2 permeation. CO_2 seems to permeate through a very small amount of larger structural defects. The observed H_2/CO_2 separation selectivity was higher than ideal selectivity, implying the larger defects are also selective for H_2 over CO_2, likely due to the smaller size of H_2. H_2/CO_2 separation selectivity decreased with the increase of temperature, resulting from the faster increase of CO_2 permeance than that of H_2. But, even at 100 ^oC, H_2/CO_2 selectivity was still 250 for the 18-nm thick membrane. This suggests a more activated CO_2 diffusion than H_2 through GO membranes, resulting from the tight fit of CO_2 molecules in these defects (*13*). H_2/N_2 mixture separation showed a similar behavior, and the highest selectivity is approximately 900 for the 9-nm GO membrane at 20 ^oC. We have prepared at least 3 GO membranes for each thickness and obtained good reproducibility; variation of membrane permeation performance is within 15% for all membranes. We also fabricated ultrathin GO

membranes on low-cost polycarbonate supports (100-nm pores) and obtained similar separation performance. For example, for a ca. 18-nm thick GO membrane on polycarbonate support, H_2/CO_2 and H_2/N_2 separation selectivities are 1,110 and 300, respectively. Figure 2.9G shows a comparison of ultrathin GO membranes with polymeric membranes and inorganic membranes for H_2/CO_2 mixture separation. Typically, for membrane separation, as separation selectivity increases, permeance decreases. An upper bound can usually be used to compare the separation performance of a new membrane with previous membranes. Ultrathin GO membranes are far above the upper bounds for both polymeric membranes (black line) and representative inorganic membranes (red line). Figure 2.11 also shows the comparison of GO membranes with polymeric membranes for H_2/N_2 mixture separation; superior separation performance of GO membranes can again be seen.

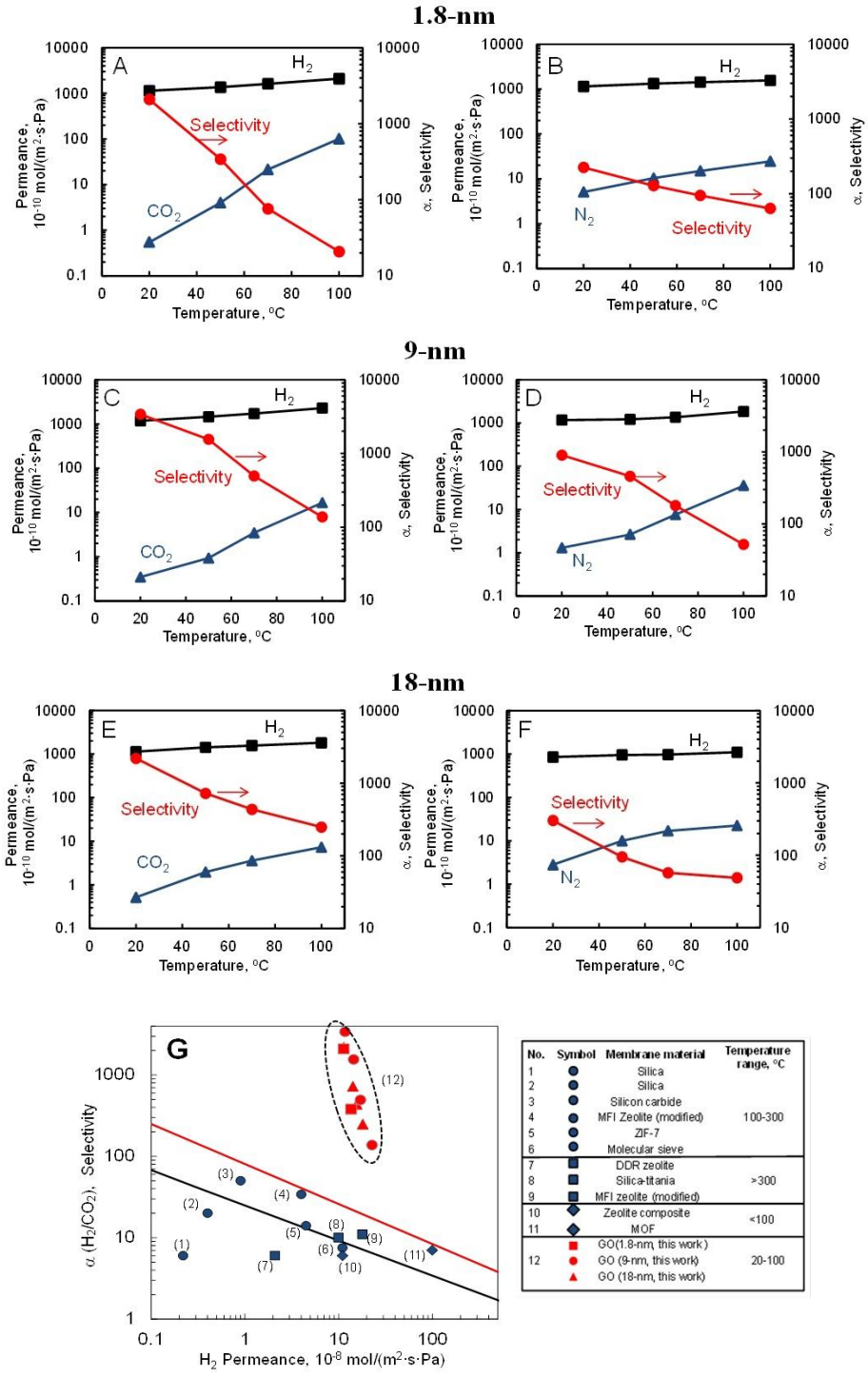

Figure 2. 9 50/50 H_2/CO_2 and H_2/N_2 mixture separation by ultrathin GO membranes and comparison with membranes in the literature for H_2/CO_2 mixture separation. (A) and (B) are separation results for 1.8-nm thick GO membrane, (C) and (D) for 9-nm membrane, and (E) and (F) for 18-nm membrane. (G) Comparison of ultrathin GO membranes with polymeric membranes and inorganic microporous membranes for H_2/CO_2 mixture separation: selectivity versus H_2 permeance. Black line is the 2008 upper bound of

polymeric membrane for H_2/CO_2(*27*), assuming membrane thickness is 0.1 m. Blue points (1-11) are microporous inorganic membranes from the literature (*28*), and the red line is the upper bound for inorganic membranes, based on blue points. Red points (12) are ultrathin GO membranes from this study. The table next to (G) explains points (1-12).

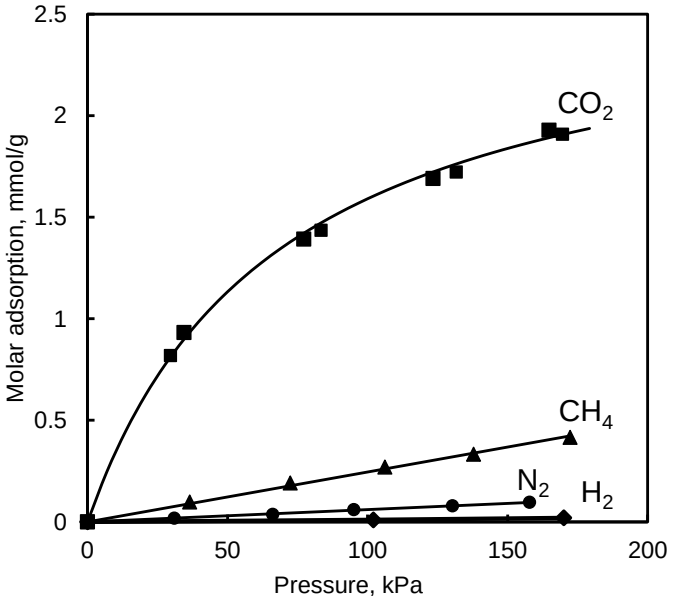

Figure 2. 10 Gas adsorption isotherms of CO_2, CH_4, N_2, and H_2 on GO at 20 ^oC

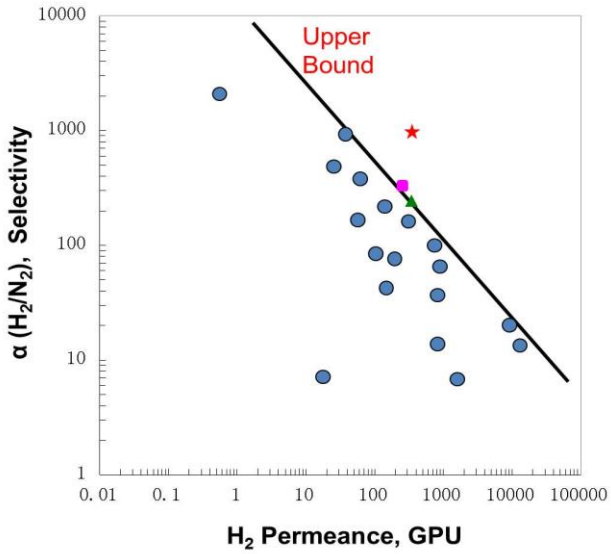

Figure 2. 11 Comparison of ultrathin GO membranes with polymeric membranes for H_2/N_2 mixture separation at 20 ^oC: selectivity versus H_2 permeance. Black line is the 2008 upper bound of polymeric membranes for H_2/N_2(*27*), assuming membrane thickness

is 0.1 μm. Blue solid spheres are representative points for polymeric membranes from the literature (*27*); green solid triangle, solid red star, and solid pink square are for 1.8-, 9-, and 18-nm GO membranes. 1 GPU (Gas Permeance Unit) equals to 3.348×10^{-10} mol/(m^2·s·Pa).

2.4 Supporting Information

2.4.1 Materials and Methods

Graphene Oxide (GO) membrane fabrication and reduction

We used single-layered graphene oxide (SLGO) powder, prepared by the Modified Hummer's Method, as the raw material for membrane preparation. We purchased SLGO from CheapTubes Inc. Firstly, SLGO powder was dissolved in DI water, followed by a 25 min sonication (Branson 2510). Then, the dispersed SLGO powder was centrifuged at 10,000 rpm for different times (Bio Lion XC-H165) to remove large particles/aggregates in the dispersion. The concentration of the resulting SLGO dispersion was measured by UV-vis (Shimadzu UV-2010PC) with a pre-calibrated curve of GO concentration vs. absorption at 600 nm wavelength, as shown in Figure 2.3A. We investigated effects of the centrifuge time on final SLGO concentration and found that 30 and 40 min gave the same concentration, as shown in Figure 2.3B. So, for membrane fabrication, we used SLGO dispersion after 30 min centrifuge. During fabricating GO membranes, we used the SLGO dispersion to do vacuum filtration (Millipore filtration system) through anodic aluminum oxide (AAO) filters with 20-nm pores (Whatman) or isopore cellulous acetate with 100-nm pores (Millipore). To roughly control the GO membrane thickness, we calculated the effective filtration area and added the known amount of GO in its 25-ml dispersion for filtration, assuming the membrane density is similar to that of graphite (~2.1 g/cm^3). The actual thickness of a thick GO membrane

with known amount of GO was measured by FE-SEM (Figure 2.4G) and used to calculate thickness of thinner GO membranes with much smaller amount of GO. The resulting GO membranes were stored in a vacuum desiccator (Nalgene) for >15 hours to remove the residue water before permeation test. A schematic process of the fabrication steps is shown in Figure 2.1. Reduced GO (rGO) membranes were fabricated in both H_2 and vacuum at 220 ^{o}C. For H_2 rGO membranes, reduction was conducted in a tube furnace (Across International STF1200) at 220 ℃ for 3 h; reduction gas was composed of 5% H_2 and 95% Ar, and temperature ramp rate was set to 5 ℃/min. For vacuum rGO membranes, GO membranes were treated in a vacuum oven (Across International VO-16020) for 19 h at 220 ℃.

Permeation/separation experimental setup

A glass membrane module was used for gas permeation/separation experiments. Silicon O-rings were used to seal the GO membranes on AAO supports or cellulous acetate supports. To avoid direct contact between O-rings and the GO membrane and thus potential damage on the thin GO membranes, we attached heat resistant Kapton tape with a hole on the GO membranes to expose the desired membrane area for gas permeation; a coarse filter paper (Fisher Scientific) was placed at the bottom of the AAO or cellulous acetate support to protect the support. During permeation test, feed flow was either pure gasses or gas mixtures and their composition and total flow rate were controlled by Mass Flow Controllers (Brooks 5850); on the permeate side, argon was used as a sweep gas to bring permeates into a gas chromatography (GC) for composition analysis. The reason we used argon as the sweep gas is because argon was used as the carrier gas in GC for a better detection of H_2 by thermal conductivity detector (TCD) due to their large thermal

conductivity difference. Nitrogen was detected by TCD, CH_4 and CO_2 were detected by both TCD and flame ionization detector (FID) (CO_2 as CH_4 by a methanizer). Typically, total feed flow rates were 45 sccm for single-gas permeation and 90 sccm for mixture separation, and permeate argon flow rate was 25-50 sccm. No pressure drop across the membranes was applied to avoid breaking or deforming the thin supports. Before evaluating separation performance of ultrathin GO membranes, a control experiment was first conducted for an AAO support; we found that permeances of studied gases were high ($> 10^{-6}$ mol/(m^2·s·Pa)) and ideal selectivities of H_2 over CO_2 and N_2 were low (< 5), as expected for Knudsen diffusion through 20-nm pores. A heating tape was used to heat the membrane and a temperature controller was used to control the membrane temperature, if needed. The schematic for the permeation setup is shown in Figure 2.5. For pressure driven liquid water permeation tests, we used a standard filtration system (Millipore). For a typical permeation test, pressure drop across the membrane was 70 kPa. Water flux was calculated by measuring feed side water volume change over a period of time, from several hours up to 200 hours; at least three points were measured over the permeation period to ensure water permeation was at steady state. All the measurements were conducted at room temperature.

2.4.2 Characterizations

X-ray diffraction (XRD) study of the GO powder

X-ray powder diffraction (XRD) was carried out using a Rigaku MiniFlex II diffractometer with Cu Kα radiation (λ = 0.15418 nm). The diffraction data was recorded for 2θ angles between 5 °and 60 °. XRD pattern for the GO powder was shown in Figure 2.2. The characteristic diffraction peak (002) of GO is ascribed to the introduction of

oxygenated functional groups, such as epoxy, hydroxyl (–OH), carboxyl (–COOH) and carbonyl (–C=O) groups attached on both sides and edges of carbon sheets (*27*).

X-ray photoelectron spectroscopy (XPS) analysis of GO membranes

The surface chemical compositions of GO membranes with different thickness (1.8, 9 and 18 nm) was analyzed by XPS (Kratos Axis Ultra DLD instrument equipped with a monochromated Al Ka x-ray source and hemispherical analyzer capable of an energy resolution of 0.5 eV), as shown in Figure 2.4H and I. The Al 2p peak appears near 74.3. For C 1s, 284.5 eV corresponds to the C-C, C=C and C-H bonds. 286.5 eV and 288.3 eV are assigned to C-O and C=O, respectively. We calculated the kinetic energy for Al 2p electrons with the equation $E_{kinetic} = E_{X\text{-}ray\ photon} - E_{binding} - \Phi$, where $E_{X\text{-}ray\ photon}$ is 1486.7 eV for Al Ka x-ray source, $E_{binding}$ for Al 2p electrons is 74.3 eV as shown in Figure 2.4H, and the working function Φ is 4.26 eV. Thus the kinetic energy for Al 2p electrons is 1408.14 eV. By applying the dependence of inelastic mean free path (IMFP) for electrons on their kinetic energy (*28*), we get the λ_{IMFP} around 3.4 nm, which is larger than the thickness of our 1.8 nm GO membrane. Similarly, for C 1s electrons, λ_{IMFP} in carbon is approximately 3 nm, which is smaller than the thickness of both 9 and 18 nm GO membrane. This is why as the membrane thickness increases, C 1s peak intensity increases, while Al 2P peak intensity decreases, and for 9 and 18 nm GO membranes on AAO, Al 2p and C 1s spectra are similar.

Atomic force microscopy (AFM) study of GO flakes

To prepare samples for AFM imaging, 0.002 mg/mL GO suspensions were first diluted 1000 times. A 4 uL drop of diluted suspension was deposited onto freshly cleaved muscovite mica disks (9.9 mm diameter, Grade V1, Structure Probe, Inc.) and dried for at

least 20 mins at 323K prior to AFM imaging. The deposited GO sheets were imaged using a PicoPlus AFM (Agilent) operated in the tapping mode. All images were collected using N-type silicon cantilevers (FORTA-50, Nanoscience Instruments, Inc.) with spring constants of 1.2-6.4 N/m, resonance frequencies of 47-76 kHz, and nominal tip radius of < 10 nm. The height resolution of the AFM scanner is less than 1 A. Thus, with proper calibration, the accuracy of the measured height of surface features is approximately ±0.1 nm. The AFM topography images were analyzed using image analysis software (Scanning Probe Image Processor or SPIP, Image Metrology A/S, Denmark), as shown in Figure 2.4B. It is seen that the GO sheet is a typical single-layer GO flake with a dimension of 300-700 nm. The GO flake showed a smooth planar structure. The height profile diagram Figure 2.4C of the AFM image showed that the thickness of the single-layer GO sheet was 0.7-0.9 nm, which is consistent with the 0.8 nm as the typical thickness of the observed single-layer GO (*29*).

Field emission scanning electron microscopy (FE-SEM) study of the GO membranes

Figure 2.4E and F show the FE-SEM (Zeiss Ultraplus Thermal Field Emission Scanning Electron Microscope) images for blank AAO and 18 nm GO membranes coated on AAO, respectively. The difference between coated and uncoated AAO can be easily noticed that for uncoated AAO, there are 20 nm pores all around the surface dispersed uniformly, while for the coated AAO with thin layers of GO on the top, the AAO intrinsic 20 nm pores are covered by GO layers. A cross-section image for our 180 nm thick GO membrane on AAO support is shown in Figure 2.4G.

Gas adsorption isotherms study on GO powder

Adsorption isotherms of CO_2, CH_4, N_2 and H_2 on GO powder were measured by a volumetric method using a home-built adsorption system. GO powder (~0.5 g) was firstly outgassed at 80-100 ^oC overnight. Helium was then used to calibrate the volume of adsorption cell with GO powder at 20 ^oC. After vacuum to remove residue gasses in the adsorption system, interested gases were introduced at 20 ^oC to measure the adsorption isotherms on GO. The operating pressure range is from 0 to 170 kPa.

High-resolution transmission electron microscopy (HRTEM) study of the GO flakes

To find out the defects on the single-layer GO sheets, we conducted HRTEM (JEOL JEM 2100F HRTEM). Figure 2.12 shows a HR-TEM of a GO flake. Under the current resolution, no conclusive evidence shows obvious defects on GO flakes, although Raman spectrum suggests the existence of defects on GO (see analysis below).

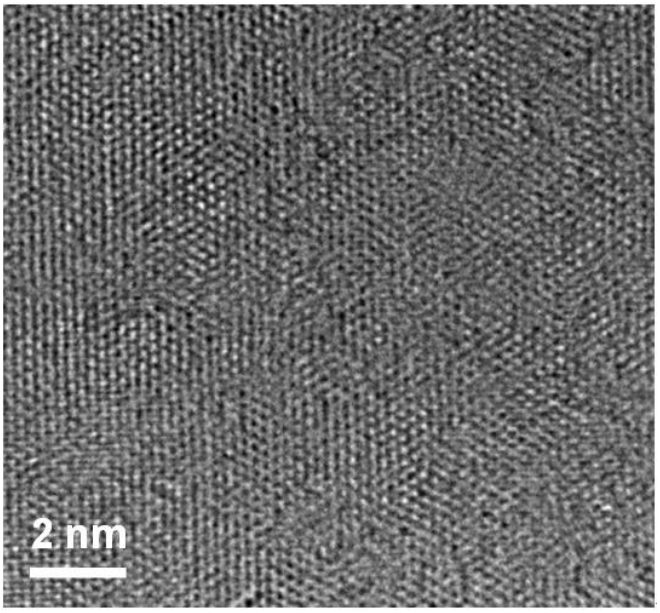

Figure 2. 12 HR-TEM image of a GO flake

Raman spectroscopy analysis of GO powder

To further study the structural properties of the GO powder, we conducted Raman spectroscopy. A LabRam confocal Raman spectrometer (JY Horiba) is used for the measurement. The spectrometer is equipped with a liquid-nitrogen cooled, charge-coupled device (CCD) detector, and a He-Ne (632.817 nm) laser for excitation. The well-known Raman characteristics of carbon materials are the G and D bands (1580 and 1350 cm^{-1}) which are usually assigned to the graphitized structure and local defects/disorders particularly located at the edges of graphene and graphite platelets, respectively (*30*) (*31*). Therefore, a smaller I_D/I_G peak intensity ratio can be assigned to lower defects/disorders in the graphitized structure. The Raman spectrum shown in Figure 2.8 displays the G band at 1585 cm^{-1} and the D band at 1338 cm^{-1}. The values of the I_D/I_G ratio were also obtained and presented in Figure 2.8. Cançado (*32*) developed a methodology to correlate the I_D/I_G ratio with the distance between pointlike defects (L_D) on single layer graphene (SLG), focusing on the low-defect density regime ($L_D \geqq 10$ nm), as shown in the following equation.

$$L_D^2\ (\mathrm{nm}^2) = \frac{(4.3 \pm 1.3) \times 10^3}{E_L^4}\left(\frac{I_D}{I_G}\right)^{-1}$$

By substitute $I_D/I_G = 1.09$ and $E_L = 1.96$ eV for the He-Ne (632.817 nm) laser into this equation, we can get the L_D between 13.6 to 18.6 nm, assuming this dependence of I_D/I_G on L_D can also be applied to SLGO. The detailed derivation of this equation can be found in ref (*32*).

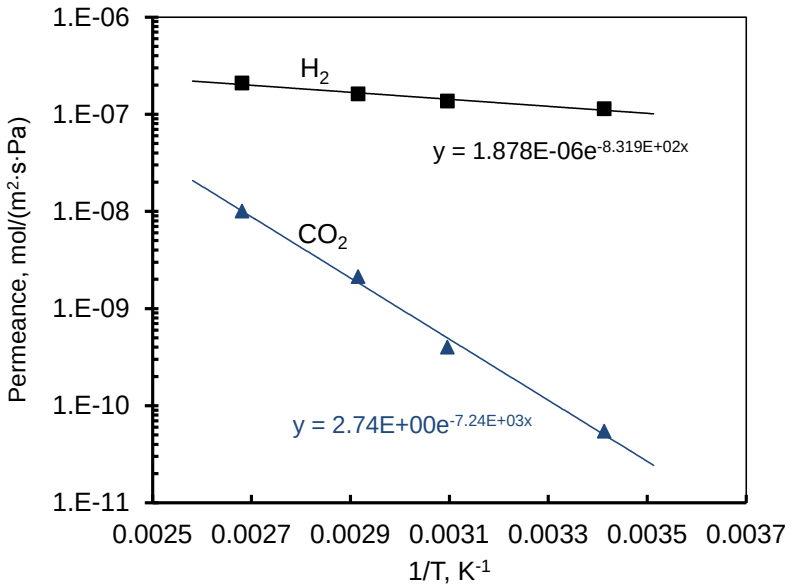

Figure 2. 13 Arrhenius temperature dependence of H_2 and CO_2 permeances in the 50/50 mixture for the1.8-nm thick GO membrane. Gas permeance through the membrane satisfies Arrhenius dependence when adsorption is in Henry's region (*35*):

$$Permeance \propto e^{\frac{-(E_d - \Delta H_{ads})}{RT}}$$

where, E_d is diffusion activation energy (kJ/mol) and ΔH_{ads} is the heat of adsorption (kJ/mol). From the above figure, the calculated (E_d - ΔH_{ads}) are 6.9 kJ/mol for H_2 and 60.2 kJ/mol for CO_2, respectively. Considering much weaker adsorption of H_2 on most of porous materials than CO_2, heat of adsorption of CO_2 on GO is also expected to be higher than H_2. Therefore, diffusion activation energy of CO_2 through the GO membrane is at least 53.3 kJ/mol higher than that of H_2, indicating much more activated diffusion of CO_2 through GO membranes or much tighter fit of CO_2 in defects of GO flakes.

2.5 Conclusion

In summary, gas separation membranes, down to 1.8 nm in thickness, were reproducibly fabricated by a scalable method. These membranes showed H_2/CO_2 and H_2/N_2 mixture separation selectivities that are 1-2 orders of magnitude higher than the state-of-the-art microporous membranes. The fabrication of membranes on a low-cost polymer support was also demonstrated, making them attractive for the practical H_2 separation from mixtures.

2.6 Acknowledgments

We acknowledge support from USC start-up funding and experimental assistance on XPS and Raman Spectroscopy by Shuguo Ma and Dr. Christopher T. Williams, respectively. We will also thank Dr. John R. Regalbuto for suggestions on writing the manuscript.

2.7 References

1. Z. P. Lai *et al.*, *Science* **300**, 456 (2003).

2. M. Yu, R. D. Noble, J. L. Falconer, *Acc. Chem. Res.* **44**, 1196 (2011).

3. R. M. de Vos, H. Verweij, *Science* **279**, 1710 (1998).

4. M. B. Shiflett, H. C. Foley, *Science* **285**, 1902 (1999).

5. H. B. Park *et al.*, *Science* **318**, 254 (2007).

6. D. A. Dikin *et al.*, *Nature* **448**, 457 (2007).

7. S. S. Chen *et al.*, *ACS Nano* **5**, 1321 (2011).

8. C. Lee, X. D. Wei, J. W. Kysar, J. Hone, *Science* **321**, 385 (2008).

9. J. S. Bunch *et al.*, *Nano Lett.* **8**, 2458 (2008).

10. R. R. Nair, H. A. Wu, P. N. Jayaram, I. V. Grigorieva, A. K. Geim, *Science* **335**, 442 (2012).

11. O. Leenaerts, B. Partoens, F. M. Peeters, *Applied Physics Letters* **93**, 193107 (Nov 10, 2008).

12. S. P. Koenig, L. Wang, J. Pellegrino, J. S. Bunch, *Nature Nanotechnol.* **7**, 728 (2012).

13. See Supplementary Material.

14. S. T. Oyama, D. Lee, P. Hacarlioglu, R. F. Saraf, *J. Membr. Sci.***244**, 45 (2004).

15. D. E. Jiang, V. R. Cooper, S. Dai, *Nano Lett.* **9**, 4019 (2009).

16. H. L. Du *et al.*, *J. Phys. Chem. C* **115**, 23261 (2011).

17. X. Qin, Q. Y. Meng, Y. P. Feng, Y. F. Gao, *Surf. Sci.* **607**, 153 (2013).

18. N. W. Ockwig, T. M. Nenoff, *Chem. Rev.* **107**, 4078 (2007).

19. P. Bernardo, E. Drioli, G. Golemme, *Ind. Eng. Chem. Res.* **48**, 4638 (2009).

20. A. Brunetti, F. Scura, G. Barbieri, E. Drioli, *J. Membr. Sci.* **359**, 115 (2010).

21. C. A. Scholes, K. H. Smith, S. E. Kentish, G. W. Stevens, *Int. J. Greenhouse Gas Control* **4**, 739 (2010).

22. M. Hong, S. G. Li, J. L. Falconer, R. D. Noble, *J. Membr. Sci.* **307**, 277 (2008).

23. G. Q. Guan, T. Tanaka, K. Kusakabe, K. I. Sotowa, S. Morooka, *J. Membr. Sci.* **214**, 191 (2003).

24. T. Tomita, K. Nakayama, H. Sakai, *Micropor. Mesopor. Mater.* **68**, 71 (2004).

25. L. M. Robeson, *J. Membr. Sci.* **320**, 390 (2008).

26. Y. S. Li, F. Y. Liang, H. G. Bux, W. S. Yang, J. Caro, *J. Membr. Sci.* **354**, 48 (2010).

27. H. K. Jeong *et al.*, *J. Am. Chem. Soc.***130**, 1362 (2008).

28. A. Kolmakov *et al.*, *Nature Nanotechnol.* **6**, 651 (2011).

29. H. C. Schniepp *et al.*, *Journal of Physical Chemistry B* **110**, 8535 (2006).

30. A. C. Ferrari, J. Robertson, *Phys. Rev. B* **61**, 14095 (2000).

31. D. Graf *et al.*, *Nano Lett.* **7**, 238 (2007).

32. L. G. Cancado *et al.*, *Nano Lett.* **11**, 3190 (2011).

33. M. S. Strano, H. C. Foley, *Carbon* **40**, 1029 (2002)

CHAPTER 3: GRAPHENE OXIDE MEMBRANES WITH HIERARCHICAL ROUGHNESS FOR HIGH FLUX, ANTI-FOULING OIL/WATER SEPARATION

3.1 Abstract

Fouling of nano/ultrafiltration membranes in oil/water separation is a longstanding issue and a major economic barrier for their wide application. Currently reported membranes typically show severe fouling, resulting from the strong adhesion of oil on membrane surface and/or oil penetration inside the membranes. This greatly degrades their performance and shortens service lifetime. Here, we report, for the first time, the use of graphene oxide (GO) for the fabrication of fully-recoverable membranes for high flux, antifouling oil/water separation via function and structure mimicking of fish scales. The ultrathin, amphiphilic, water-locking GO coating mimics the thin mucus layer covering fish scales, while the combination of corrugated GO flakes and intrinsic roughness of the porous supports successfully reproduces the hierarchical roughness of fish scales. Cyclic membrane performance evaluation tests revealed ~100% membrane recovery by facile surface water flushing, establishing their excellent easy-to-recover capability. This new generation of functional coatings/membranes may have wide applications in oil-polluted environments.

One Sentence Summary: Graphene oxide membranes/coatings with hierarchical surface roughness fully mimic function and structure of fish scales and achieve excellent anti-fouling performance in oil/water separation.

3.2 Introduction

Underwater superoleophobic surfaces have shown increasing importance in a variety of applications among which oil/water separation is of great interest due to the increasing amount of oily wastewater from industries, a shortage of clean water, and frequent oil spill accidents [1-4]. Despite recent advances in nano/ultrafiltration membranes in oil/water separation, fully recoverable oil/water separation performance has rarely been demonstrated, especially for stable, difficult-to-separate oil emulsions. A promising strategy of designing superoleophobic surfaces for underwater applications is to incorporate desirable hierarchical surface roughness[5], as inspired by the natural formation of fish scales[6-8]. Mimicking the structure of fish scales has been attempted to for the preparation of superoleophobic surfaces and has been studied for oil/water separation. Compared with conventional antifouling coating agents[2], bio-inspired underwater superoleophobic materials have improved oil/water separation performance and enhanced fouling resistance[9-13]. Most previous studies, however, focused merely on replicating the structure of fish scales. The function of the mucus layer on the surface of fish scales was usually neglected. In fact, the mucus layer replicates the hierarchical roughness of the fish scales underneath, and it preferentially attracts water molecules in oil/water mixtures, forming a superoleophobic oil/water/solid interface. To mimic the excellent anti-fouling and self-cleaning performance of fish scales, a combination of the hierarchical surface roughness and the conformal, underwater superoleophobic coating

layer is apparently necessary. However, it is highly challenging to perfectly combine these two aspects, and little success has been reported to date. Graphene oxide (GO) is a promising two-dimensional (2-D) membrane/coating material, owing to its one carbon atom thickness, ease of conformation to substrates, excellent chemical stability[14], and mechanical strength[15]. GO membranes have shown great potential for gas and liquid separations through size-sieving by either interlayer spacing or selective structural defects[16-21]. Here, we report, for the first time, the utilization of mucus-mimicking GO for fabricating ultrafiltration membranes with desirable hierarchical surface roughness and their application for high flux, anti-fouling oil/water separation.

3.3 Experimental Results and Discussion

We first used single-layered GO (SLGO) nanoflakes to prepare a free-standing GO film by vacuum filtration. The GO film is amphiphilic in air (Figure 3.1A and B) and oleophobic under water (Figure 3.1C), owing to the unique chemistry of GO [20, 22]. Functional groups, such as carboxyl, hydroxyl, and epoxy, are rich on the edges and defects, exhibiting high affinities for water molecules (Figure 3.2). The affinity of the oil droplets to smooth GO surface in air is attributed to these more hydrophobic regions in the basal GO plane[22]. Despite that oil easily spread out on the GO surface in air, we found that the interlayer structure of GO is inaccessible to oil molecules. The x-ray diffraction (XRD) patterns of GO samples before and after HD soaking showed the same characteristic *002* reflection peak at 2θ of 12.35 °(Figure 3.1D), suggesting a similar interlayer spacing (*ca.* ~0.72 nm). This result confirmed that HD cannot penetrate into the GO interlayers and swell the structure. However, the GO film was easily wetted and swelled by water molecules, leading to an increased d_{002} spacing of ~0.79 nm (calculated

based on a 2θ of 11.15°). By varying humidity, different degrees of swelling of GO structure were observed (*ca.* 0.72 nm ≤ d_{002} ≤ *ca.* 0.83 nm). We further explored the oil accessibility to a water-swollen GO sample by extending HD soaking time to 60 h. As expected, no swelling effect from HD was observed, as no further increase in d_{002} spacing was detected (Figure 3.1D). Therefore, GO well mimics the amphiphility of mucus in air and its underwater oleophobicity, and water-wetted GO has strong resistance to oil penetration.

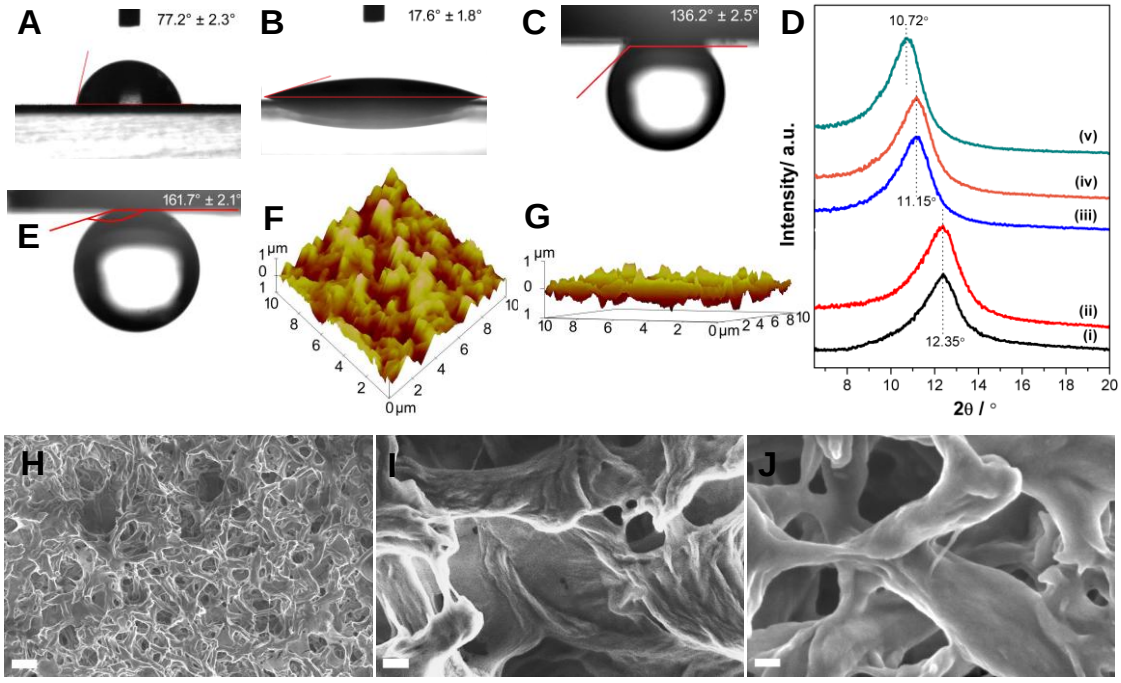

Figure 3. 1 Characterization of a free-standing GO film (thickness: 10 μm) and a 15-nm GO membrane supported on polyamide (PA). Optical images of a water droplet (**A**) and a hexadecane (HD) droplet (**B**) on the free-standing GO film in air. (**C**) Optical image of a HD droplet adhering to the free-standing GO film under water. (**D**) X-ray-diffraction (XRD) patterns of the free-standing GO film: (i) dried; (ii) soaked in HD for 30 h; (iii) soaked in water vapor for 50 h (50% humidity); (iv) soaked in HD for 60 h after (iii); and (v) soaked in saturated water vapor for 24 h; a.u., arbitrary unit. (**E**) Optical image of a HD droplet contacting with the 15-nm GO membrane in water. Atomic force microscopy (AFM) images of the top-view (**F**) and the cross-sectional view (**G**) of the 15-nm GO membrane. (**H**) Low magnification field emission scanning electron microscopy (FESEM) image of the 15-nm GO membrane surface. High magnification FESEM images of the

15-nm GO membrane on PA support (**I**) and the bare PA support (**J**). Scale bars in (H), 1 μm; in (I) and (J), 200 nm.

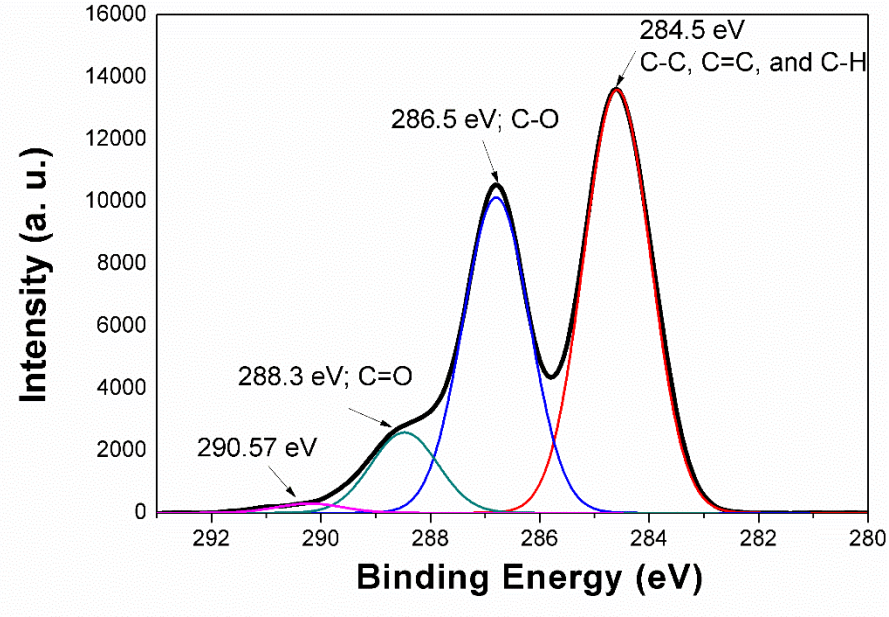

Figure 3. 2 C 1S XPS spectrum of a free-standing GO film (10 μm in thickness). a. u., arbitrary unit.

We followed a similar procedure of our previous study [19] to prepare ultrathin GO membranes/coatings on polyamide (PA) supports with large three-dimensional pores (~200 nm) to introduce a relatively large surface roughness and desirable skeleton for GO coating. Atomic force microscopy (AFM) confirmed GO flakes are single layered (Figure 3.3A and B). Figure 3.3C showed a digital image of a representative 15-nm thick (nominal thickness based on a flat surface) GO membrane on PA support with a coating area of ~9.6 cm^2. The 15-nm GO membrane exhibited a much larger underwater HD contact angle (161.7 ° ± 2.1 °) (Figure 3.1E) than the free-standing GO film with a smooth

surface (Figure 3.1C), suggesting its drastically improved oleophobicity or superoleophobicity. This can be attributed to the much rougher GO membrane surface, as discussed below. AFM image of the GO membrane surface (Figure 3.1F) showed submicron-scale roughness with an average root-mean-squared roughness (Rq) of 230.5 nm. This is comparable to that of the PA support (Rq, 240.9 nm) (Figure 3.7C and D). The cross-sectional profile (Figure 3.1G) revealed that the surface was full of micrometer-scale bumps and dents. Apparently, with the thin and conformal GO coating, the membrane preserved the original roughness of the PA support. Figure 3.1H showed the field emission scanning electron microscopy (FESEM) image of the surface of a 15-nm GO membrane. Compared with the bare PA support (Figure 3.4A), a conformal GO coating on PA skeleton can be clearly seen. More importantly, the FESEM image with higher magnification (Figure 3.1I) revealed a secondary nano-scale roughness formed by the corrugation of the flexible GO flakes, while the skeleton surface of the bare PA support was fairly smooth (Figure 3.1J). A novel membrane/coating structure with the hierarchical roughness, therefore, has been formed. Combining mucus-mimicking GO with the hierarchical roughness, we concluded that the fabricated GO membranes precisely mimicked the structure and mucus coating layer of fish scales and might have great potential to realize anti-fouling and self-cleaning performance in oil-polluted water.

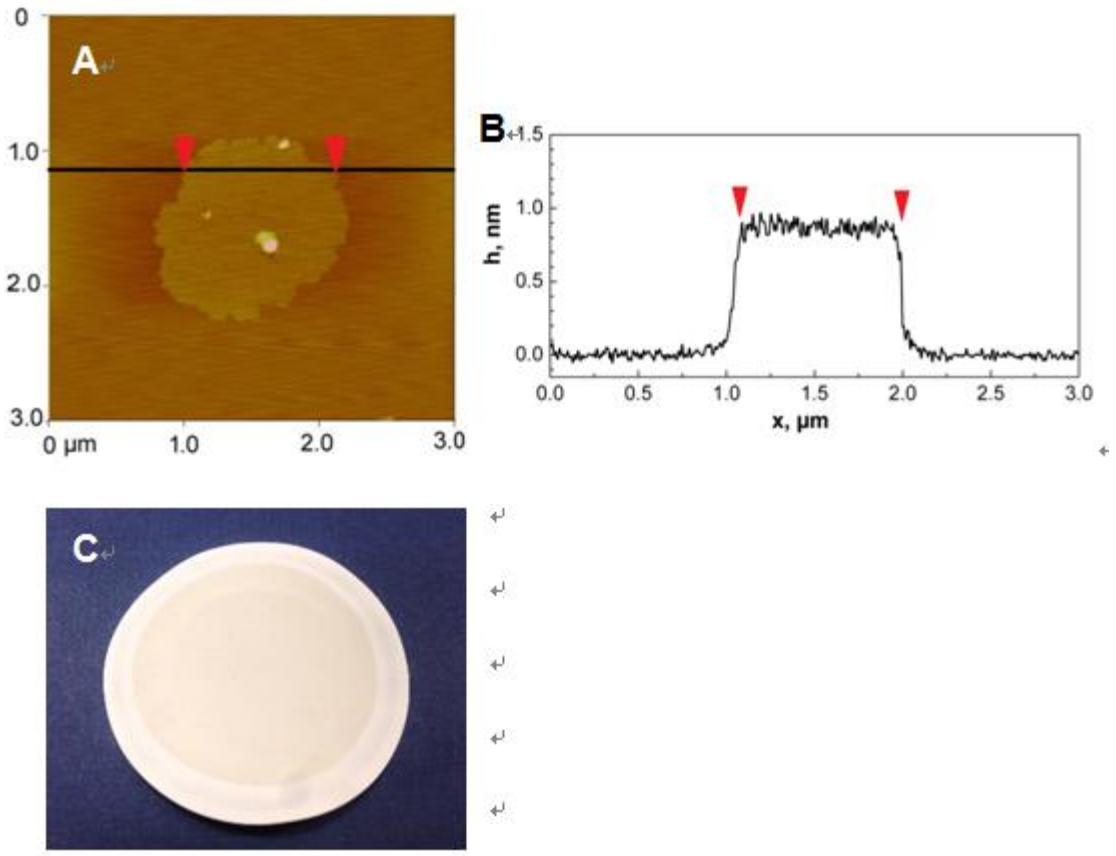

Figure 3. 3 (A) AFM topographical image of a SLGO flake on freshly cleaved mica. (B) The height profile across the black line in (A). The height data were calibrated using steps formed on freshly cleaved mica. h, height; x, position. AFM results confirmed the single-layered structure of GO of ~0.9 nm in thickness. (C) Photograph of 15-nm GO membrane (supported by porous PA). The region with light brown color reflected an active permeation area of ~9.6 cm^2.

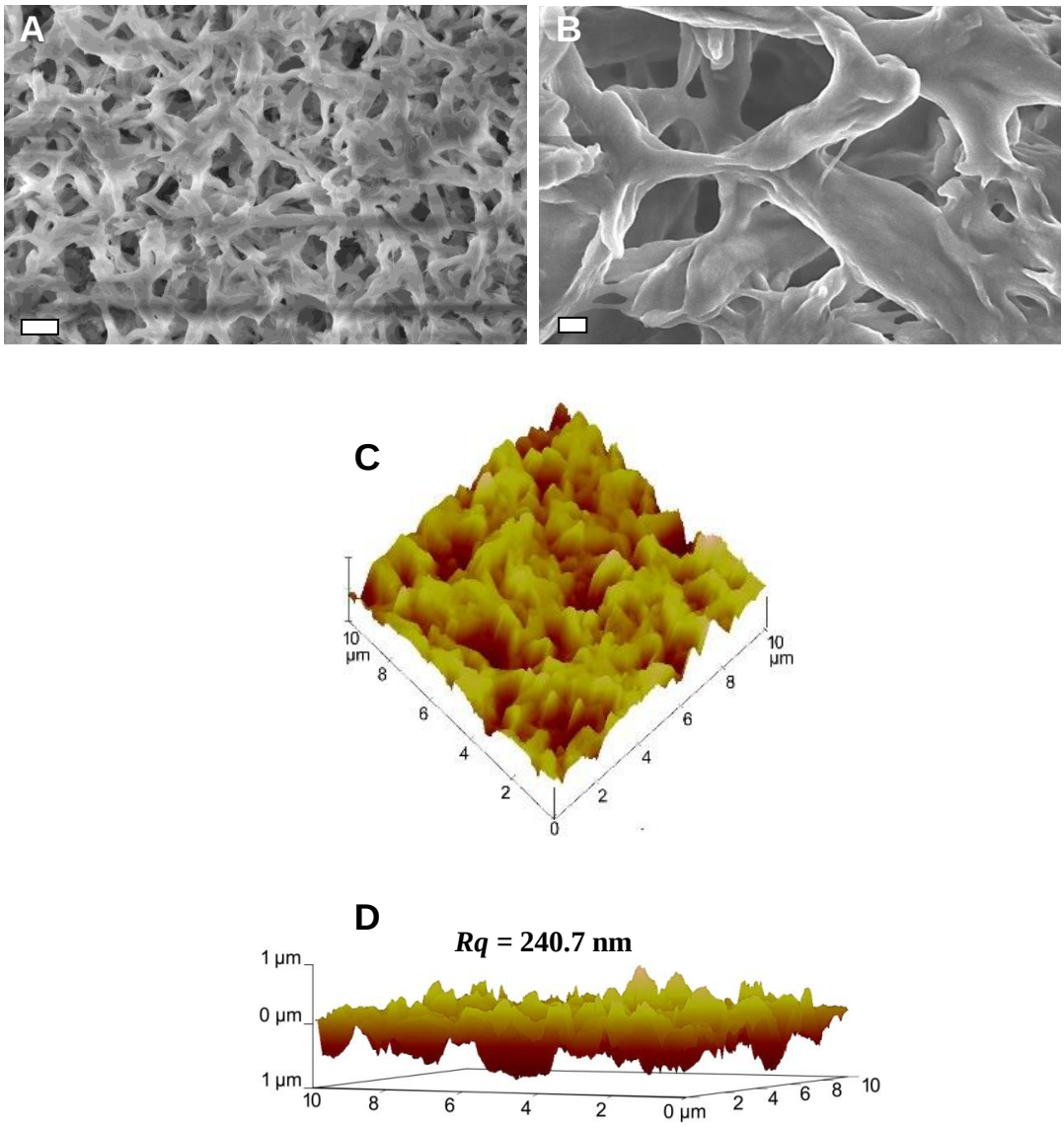

Figure 3. 4 (A) and (B) Low-voltage FE-SEM images of bare PA support in low and high magnifications, respectively. FE-SEM Image (A) showed rough porous PA surface. However, a local view (B) of the support showed PA skeleton with smooth surfaces. (C) AFM image of the support surface with an average root-mean-squared roughness (Rq) of 240.7 nm. (D) AFM image of the cross-sectional view of a 15-nm GO membrane. Scale bars, in (A) 1 µm; in (B), 100 nm.

We conducted a series of oil emulsion filtration tests using a dead-end cell filtration system (Figure 3.5) to explore the anti-fouling performance of the GO membranes. Figure 3.6A showed the performance of a 10-nm GO membrane in three cycles (also see Figure 3.7 for its characterization). Pure water flux through the fresh GO membrane was 8,100 ± 200 L/(m^2 ћ ƀar) and can be fully recovered after subsequent oil emulsion filtration cycles, exhibiting superior ease-of-recovery and anti-fouling capability. In oil emulsion separation tests, the initial flux was approximately 5,400 L/(m^2 ћ ƀar), which is 2-3 orders of magnitude higher than those of reported underwater (super)oleophobic membranes[7, 10, 23]. The initial flux was maintained in the following cycles after cleaning, confirming the full recovery of the GO membrane. A fast flux decrease was observed in the first hour. This can be attributed to the high-flux induced oil agglomeration on the membrane surface [23-25], considering more than 85 wt% of the feed was collected in the first hour. This is a well-known limitation of the dead-end filtration system. Oil rejection was as high as 98±0.1% and remained constant (Figure 3.6A). Cyclic oil-in-water emulsion separation tests were also performed on a PA support (Figure 3.6B) for comparison. Pure water flux through the fresh bare PA support was ~11,000 L/(m^2 ћ ƀar) and drastically decreased to ~1,600 L/(m^2 ћ ƀar) after the first cycle of oil emulsion filtration, and then further decreased in the following cycles. The pure water flux eventually decreased to ~1050 L/(m^2 ћ ƀar) after 2 cycles, indicating severe oil fouling. In the first oil emulsion filtration, the initial flux was only 46 L/(m^2 ћ ƀar), which was 2 orders of magnitude lower than that of the10-nm GO membrane. The flux at the end of the first cycle was as low as 15 L/(m^2 ћ ƀar), and after 2 cycles it was only 9 L/(m^2 ћ ƀar). The oil rejection was constant at 95±0.6% in each

cycle, resulting from the small pores (cutoff size of ~200 nm) of the PA support. Clearly, without GO coating, the PA support itself does not possess the anti-fouling property and recovery capability. We further increased GO membrane/coating thickness to 15 nm. Similar membrane properties and cyclic oil emulsion permeation behavior were observed (Figure 3.8), although the total flux decreased. However, the reduction of GO thickness to 5-nm led to severe fouling in the cyclic testing, apparently due to the incompletely covered PA surface by GO (Figure 3.9). Increasing GO membrane/coating thickness beyond 15 nm is expected to gradually cover PA support pores and finally eliminate hierarchical surface roughness. Indeed, for thicker GO membranes (30 and 50 nm), they lost antifouling performance and membrane fouling was seen (Figure 3.10). Based on the above results, we concluded that membrane structure and corresponding separation performance can be tailored by simply changing GO thickness. The optimization of GO membrane structures can significantly improve oil/water separation performance.

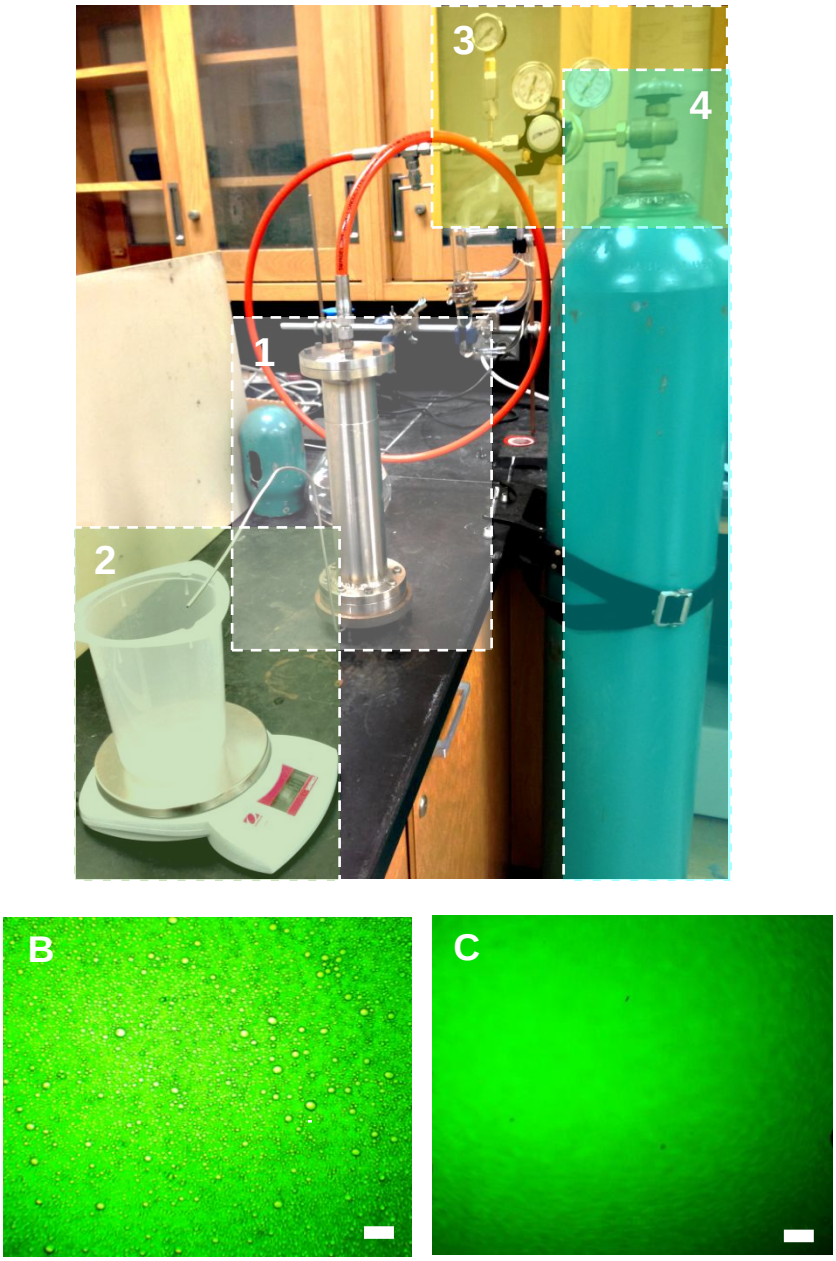

Figure 3. 5 (A) The dead-end filtration device used for cyclic membrane performance evaluation tests. The highlighted areas in the picture showed four major parts of the experimental setup. (1) Dead-end filtration system; (2) filtrate collection system; (3) pressure control system including a safety pressure relief valve; and (4) gas tank. The pressure can be applied from tens of kPa to ~50 bar. (B) Optical image of HD-in-water emulsion. The excellent stability of the emulsion was observed visually over a 24 h period, which was much longer than the time needed for the membrane experiments. The emulsions had HD particles ranging from 100 nm to 20 μm in diameter. (C) Optical image of a filtrate sample which was obtained from tests of 15-nm GO membrane. No HD droplet was observed at the same magnification, indicating high HD rejection of the membrane. Scale bars, 100 μm.

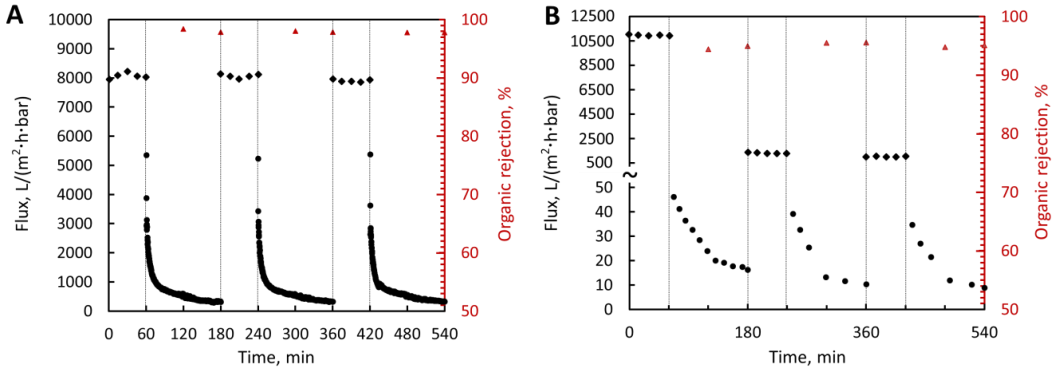

Figure 3. 6 Cyclic oil emulsion filtration tests for a 10-nm GO membrane on PA support (**A**) and bare PA support (**B**). (●) total flux in oil-in-water emulsion separation. (◆) pure water flux. (▲) total organic rejection.

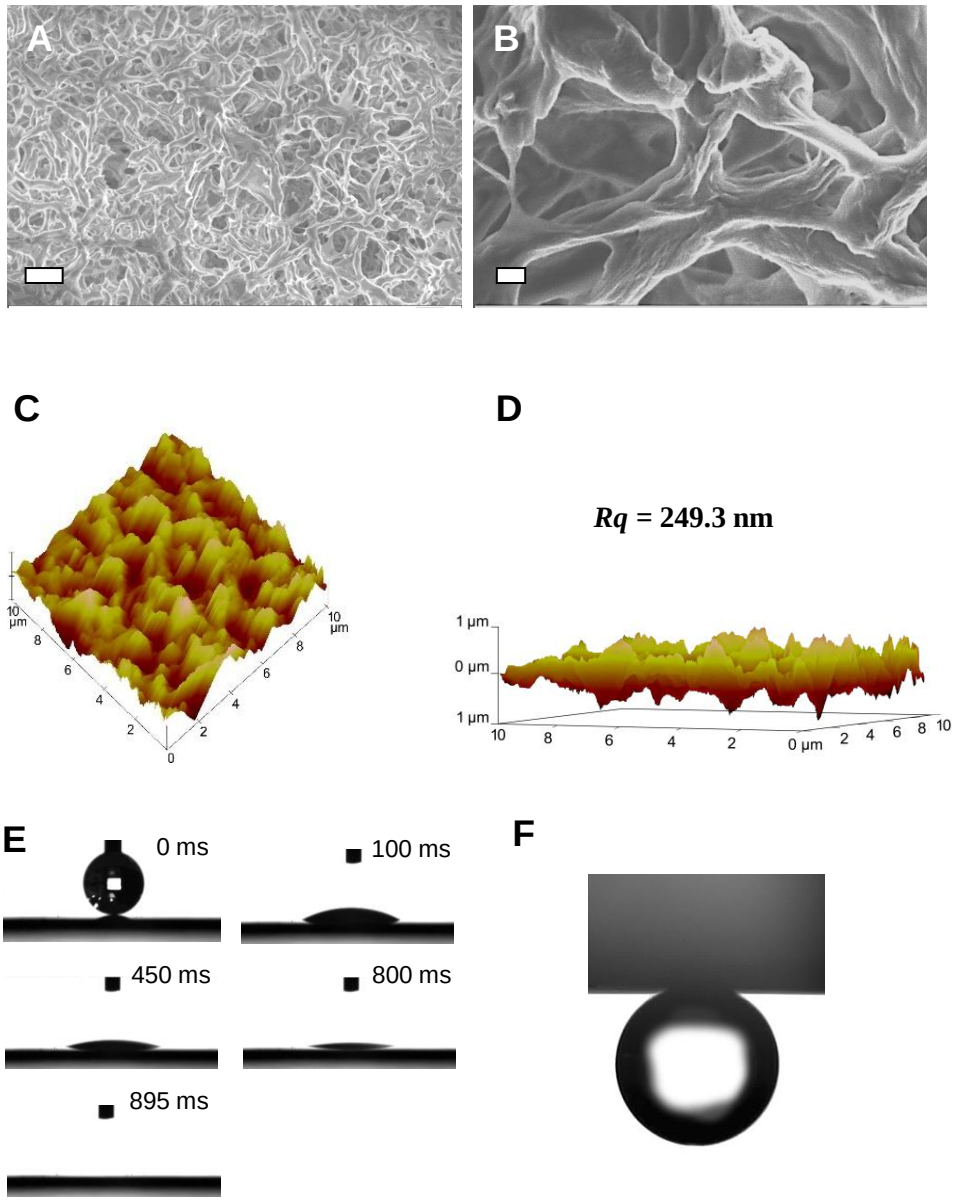

Figure 3. 7 Characterizations of a 10-nm GO membrane supported on porous PA. Low-resolution (A) and high-resolution (B) FE-SEM images of the GO membrane surface. AFM images of the top-view (C) and the cross-sectional view (D) of the GO membrane. (E) Water wettability of the membrane in air. Scale bars, in (A) 1 µm; in (B), 100 nm. (F) Optical image of a HD droplet contacting with the GO membrane surface.

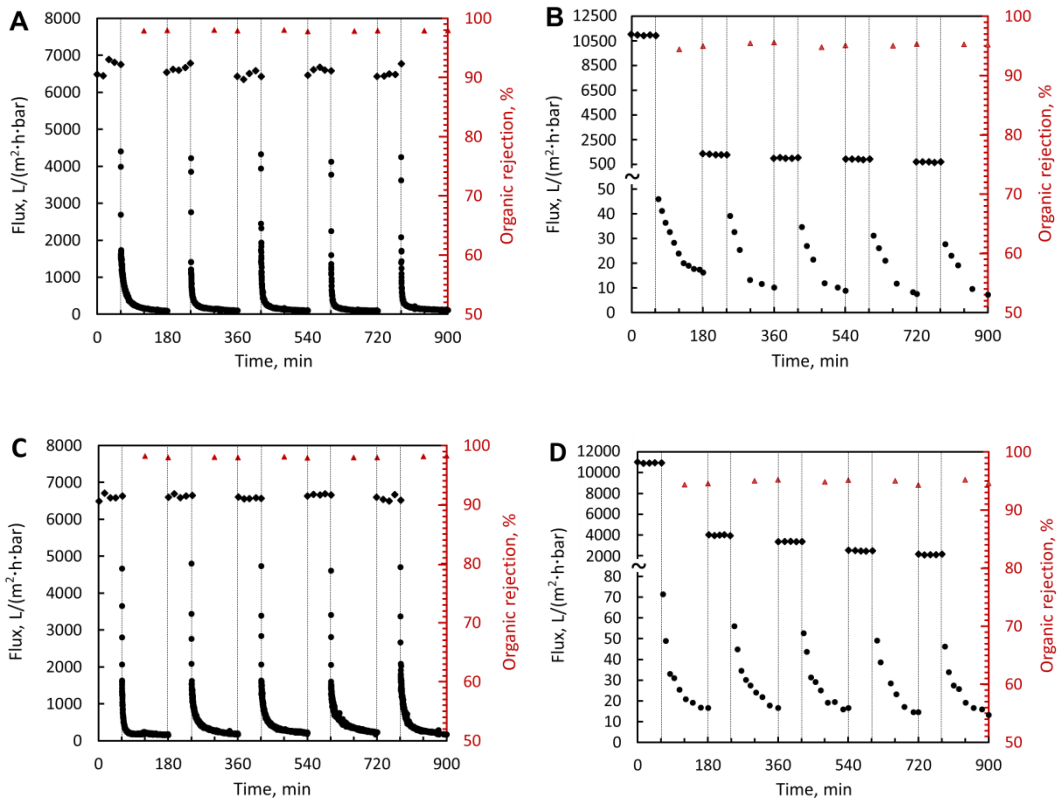

Figure 3. 8 Cyclic oil-in-water separation tests of (A) and (C) 15-nm GO membrane and (B) and (D) PA porous support. (A) and (B) HD-in-water emulsion; (C) and (D) octane-in-water emulsion.

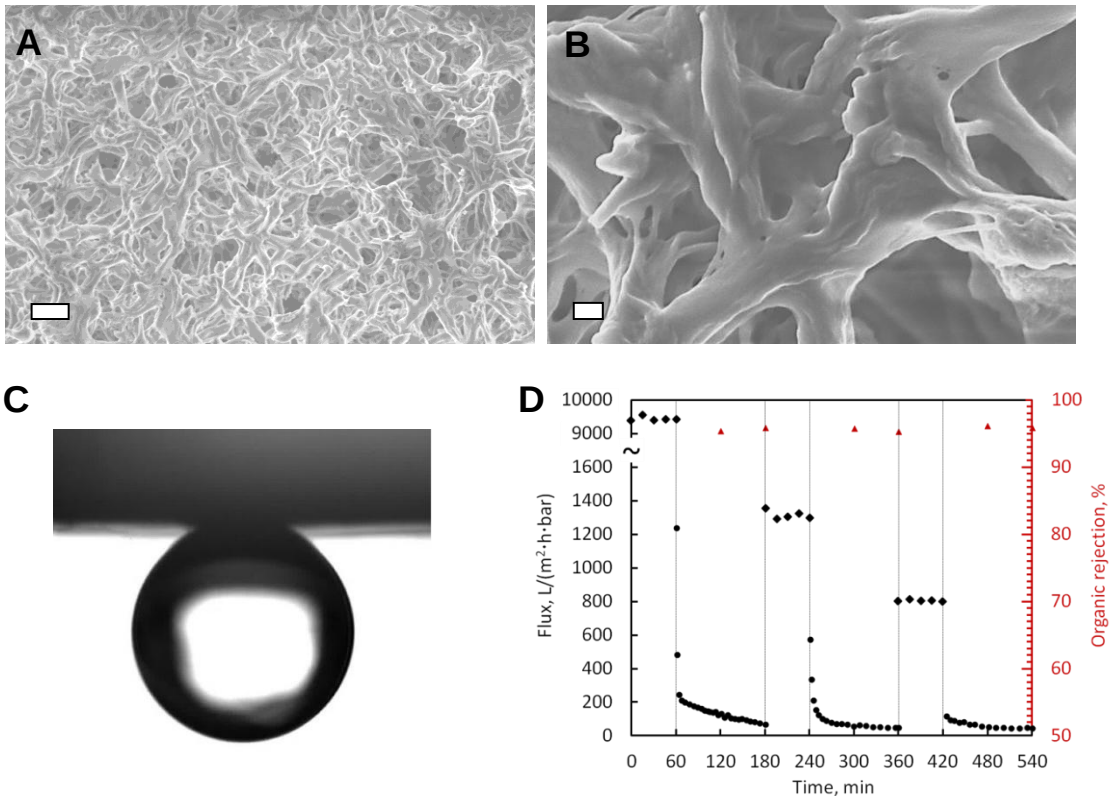

Figure 3. 9 FE-SEM images of a 5-nm GO membrane on PA support in low (A) and high (B) magnifications. (C) Optical image of a HD drop contacting with the GO surface. (D) Cyclic HD-in-water emulsion separation tests of a 5-nm GO membrane. Scale bars, in (A) 1 μm; in (B), 100 nm.

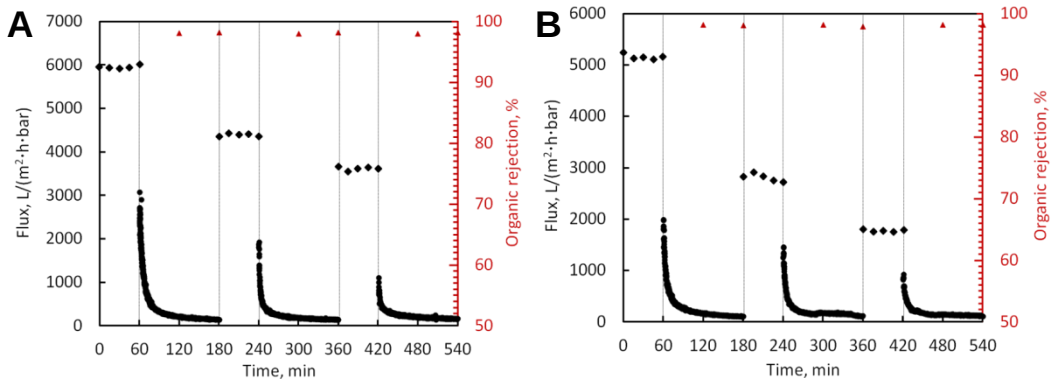

Figure 3. 10 Cyclic membrane performance evaluation tests performed on GO membranes supported by PA and AAO supports. (A) 30-nm GO on PA; (B) 50-nm GO on PA; (C) 10-nm GO on AAO; (D) bare porous AAO support.

To further understand oil separation behaviors of the GO membranes with different thicknesses, various surface characterizations were conducted (Figures 3.11 to 3.15). With the increase of the GO thickness from 30 to 80 nm, GO membranes/coatings gradually lost the intrinsic roughness of the PA support and formed continuous GO coatings on the surface (Figures 3.11 and 3.12). Also, with the increase of the GO thickness, the disappearing time of water droplets in air greatly increased, which was likely due to the degraded surface wettability and permeability (Figure 3.13). Notably, 10-nm GO showed the quickest penetration of water. Drag force tests (Figure 3.14) showed that 10-nm GO on PA had the smallest oil adhesion force, while thinner or thicker GO membranes/coatings showed much stronger oil adhesion. 10-nm GO on PA also had the largest underwater HD contact angle, while thinner or thicker GO coating had much smaller angles (Figure 3.15). All these results were consistent with the cyclic oil emulsion filtration results, suggesting 10-nm GO on PA may have the optimum hierarchical roughness. In another attempt to demonstrate the importance of the hierarchical roughness, we deposited 10-nm GO on a flat anodic aluminum oxide (AAO) support with 1-dimentional pores (20-nm pores). Again, severe membrane fouling in

cyclic oil emulsion filtration was seen (Figure 3.16). These results clearly showed the hierarchical roughness is essential for the excellent antifouling performance. We also prepared 15-nm GO on another polymeric support, cellulose nitrate (CN), with ~200-nm pores. Excellent antifouling performance was clearly seen (Figure 3.17). Figure 3.18 compared the collected water mass in the first cycle of oil emulsion filtration for GO membranes and bare supports. The collected water mass through the 10-nm GO membrane on PA support was 31, 11, and 9 times of those through the bare PA, CN, and AAO supports, respectively. Figure 3.19 showed the comparison of GO membranes with other membranes/materials reported in the literature for oil emulsion separation. Pure water flux and water flux recovery after the first oil emulsion filtration were used as two indicators of the potential productivity and anti-fouling capability, regarding to which GO membranes showed the best performance so far. All of these tests indicated the generality of the concept and the great potential of novel GO membranes/coatings with hierarchical roughness supported on a wide range of substrates for high flux, anti-fouling oil/water separation.

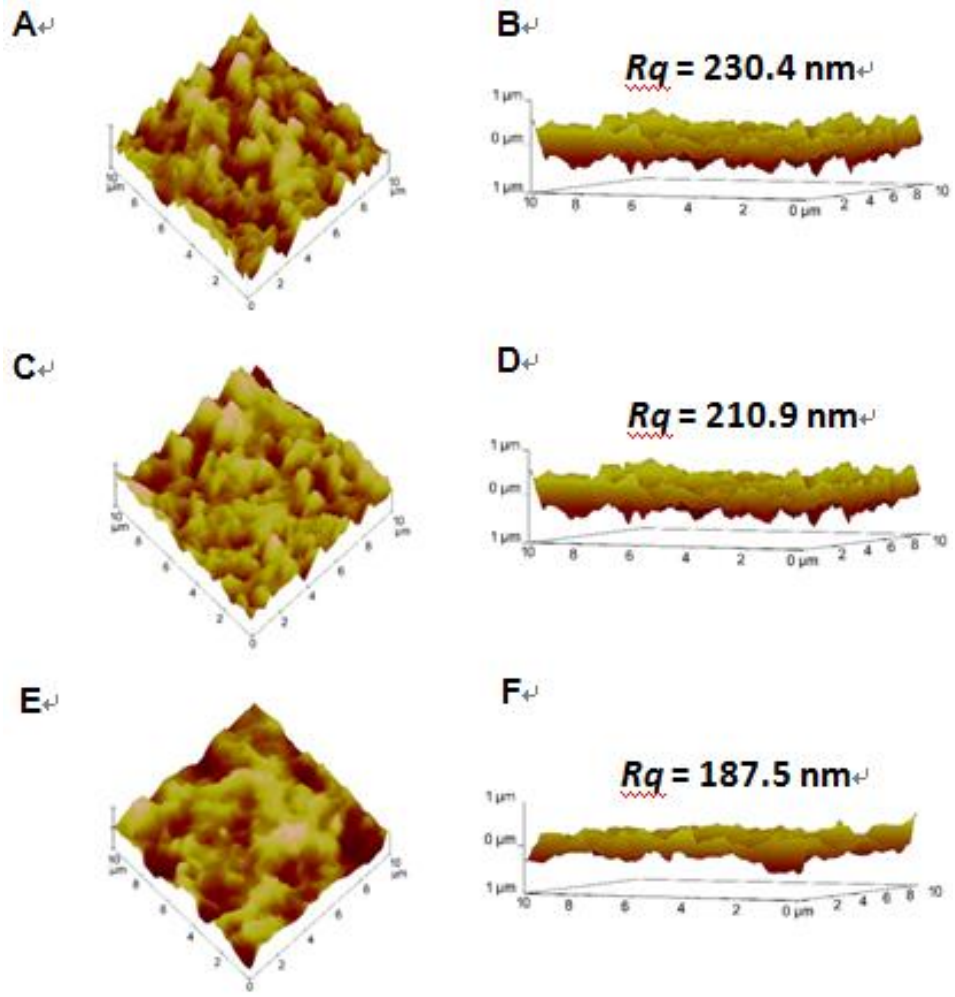

Figure 3. 11 AFM images of GO membranes. (A) and (B) 30 nm GO membrane; (C) and (D) 50 nm GO membrane; (E) and (F) 80 nm GO membrane. AFM images on the left and right hand side are top- and cross-sectional view of GO surface structure, respectively. According to AFM characterization, with the increase of GO thickness from 30 to 80 nm, the GO membranes displayed gradually decreased surface roughness.

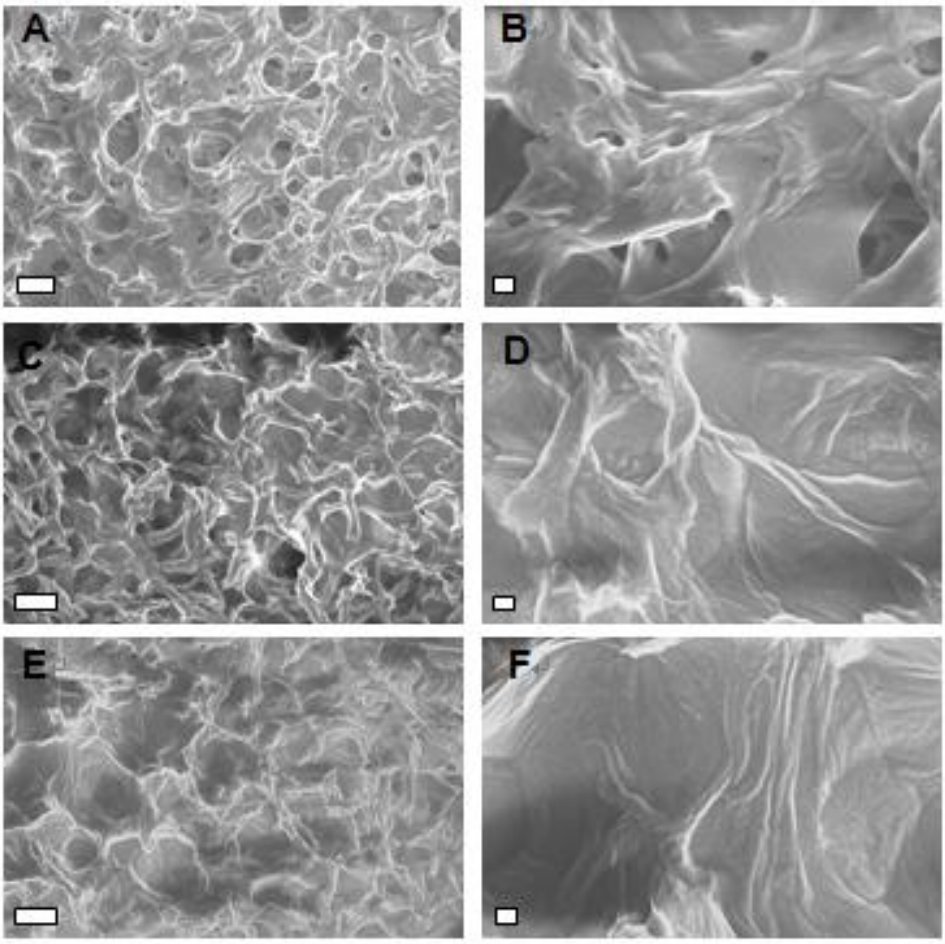

Figure 3. 12 FE-SEM images of GO membranes. (A) and (B) 30 nm GO membrane; (C) and (D) 50 nm GO membrane; (E) and (F) 80 nm GO membrane. Low and high magnification FE-SEM images were displayed on left and right hand sides, respectively. Scale bars: (A), (C) and (E), 1 μm; (B), (D) and (F), 100 nm.

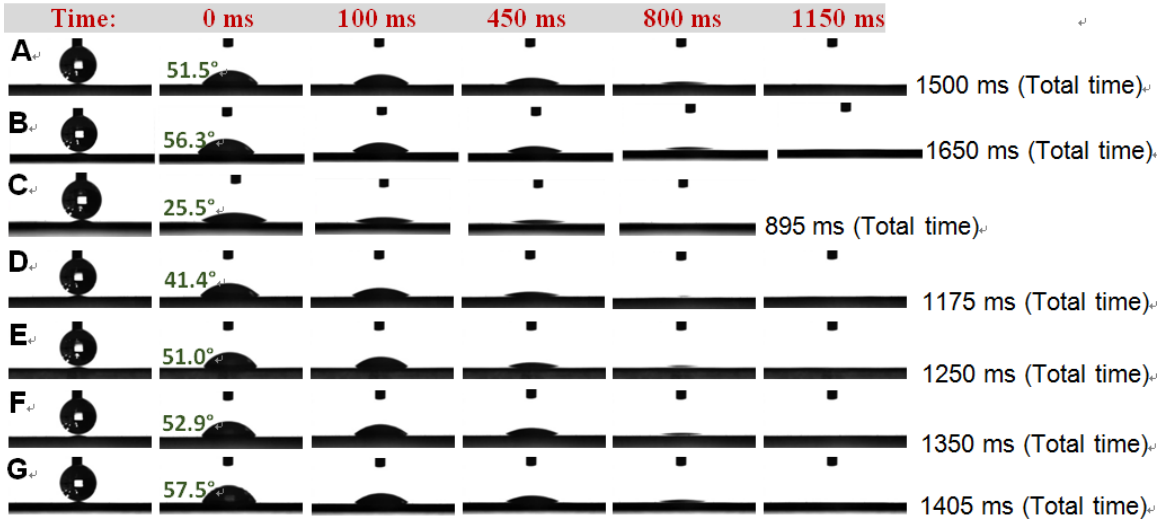

Figure 3. 13 Still optical images from video contact angle measurements of a water droplet applied on support and GO membranes. (A) Bare PA support; (B) 5-nm GO membrane; (C) 10-nm GO membrane; (D) 15-nm GO membrane; (E) 30-nm GO membrane; (F) 50-nm GO membrane; (G) 80-nm GO membrane.

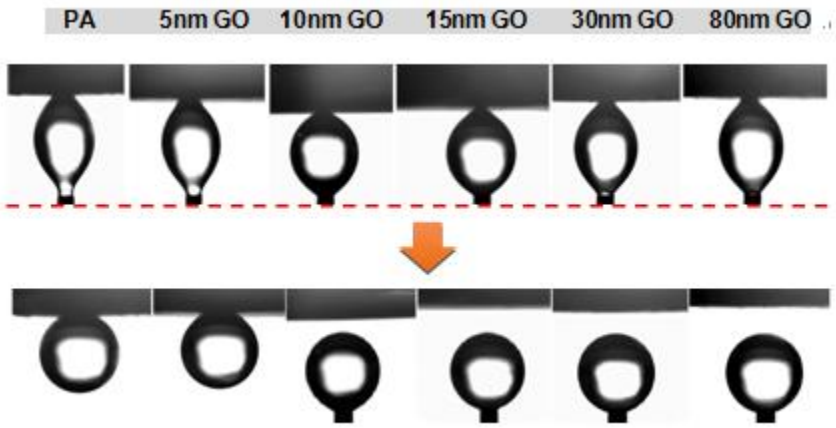

Figure 3. 14 Simulated underwater oil drag force tests. The upper images showed the largest deformation of the oil droplets before the disruption of oil/water/solid interface. The lower image showed the oil droplets can either adhere to the membrane surfaces or stay at the needle tip, depending on oil-to-surface adhesive force. The red dashed line indicated the same height of the needle tip.

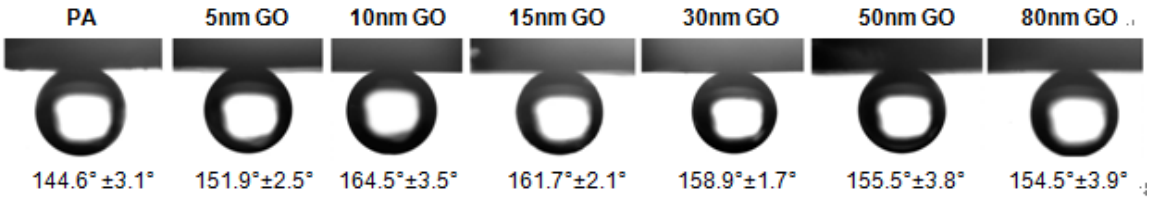

Figure 3. 15 Underwater HD contact angle measurements of GO membranes and the bare PA support.

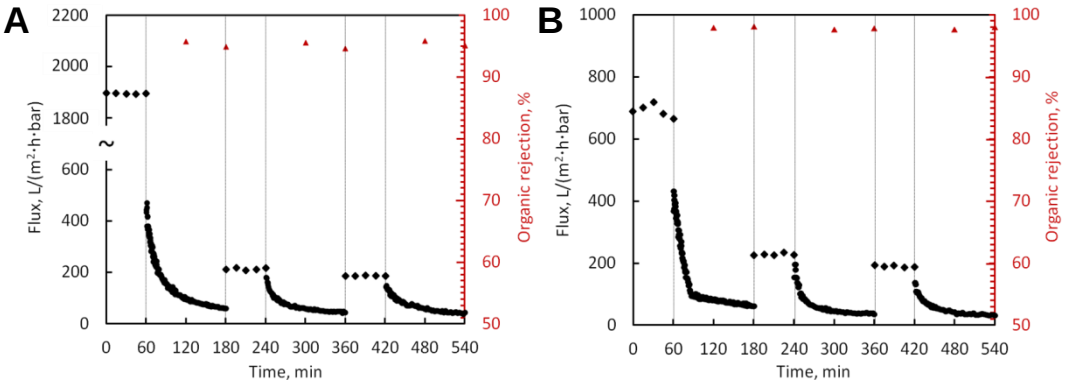

Figure 3. 16 Cyclic membrane performance evaluation tests performed on (A) bare porous AAO support; (B) 10-nm GO on AAO.

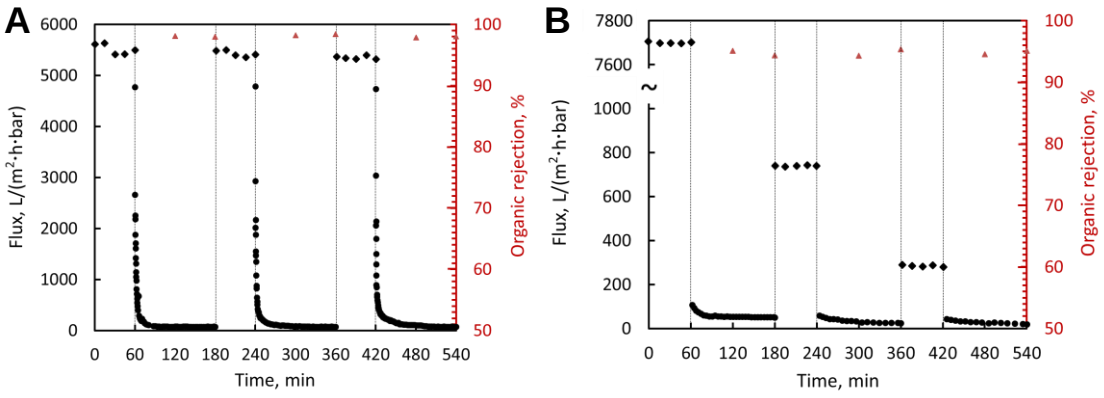

Figure 3. 17 Cyclic membrane performance evaluation tests performed on (A) 15-nm GO on porous CN and (B) bare CN support.

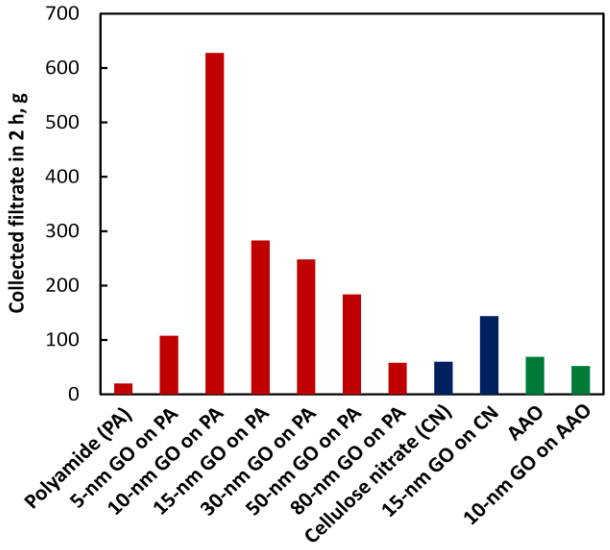

Figure 3. 18 Comparison of GO membranes/coatings with bare supports on their water production in HD-in-water emulsion filtration. Filtrate in 2 h was collected and weighed.

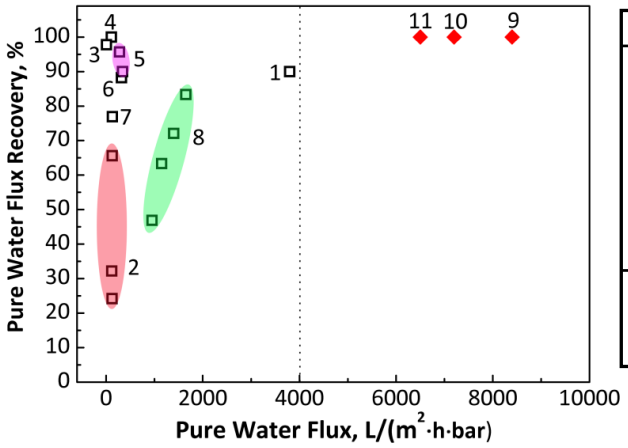

No.	Symbol	Membrane	Reference
1	□	$CaCO_3$/PAA-g-PP	[9]
2	□	PES/Pluronic F127	[24]
3	□	cellulose/NMMO·H_2O/PEG400	[26]
4	□	PAN-g-PEO	[27]
5	□	CA-g-PAN	[28]
6	□	nano-sized ZrO_2/Al_2O_3	[29]
7	□	ZrO_2/α-Al_2O_3	[30]
8	□	EVAL/PEO–PPO–PEO	[31]
9	◆	10-nm GO on PA	
10	◆	15-nm GO on CN	This work
11	◆	15-nm GO on PA	

Figure 3. 19 Comparison of GO membranes with reported oil/water separation membranes, regarding to the pure water flux of the fresh membrane and the pure water recovery after the 1st oil emulsion separation cycle. The recovery capability of the membranes is evaluated according to the equation: pure water recovery % = 100% × (ν'/ν_0); ν_0, pure water flux through a fresh membrane; ν', pure water flux after the 1st cycle of oil emulsion separation test and subsequent membrane cleaning. Note: GO membranes and the reported membranes all showed a high oil rejection >90%.

3.4 Supporting Information

3.4.1 Materials and Methods

We followed the similar procedures as described in our previous study for the preparation of GO membranes[19]. Single-layered graphene oxide (SLGO) powder was first dissolved in DI water, followed by at least 1 hour sonication (Branson 2510). The dispersion was then centrifuged (Bio Lion XC-H165) at 10000 rpm for 1 hour to remove large aggregates in the dispersion. The concentration of the resulting GO dispersion was determined by ultraviolet-visible (UV-Vis) spectroscopy (Shimadzu UV-PC2010) [see ref. 19 for the method]. GO membranes were prepared by vacuum filtration (Millipore filtration system) on porous polyamide support with 200-nm pore size (Whatman). The resulting GO membrane was left on the filtration system for 12 hours with vacuum. After that, GO membrane were ready for use. To control the thickness of GO membrane, a series of 25-mL suspensions with calculated amount of SLGO were prepared and then filtrated through the porous supports with a known effective permeation area. To test the generality of our concept of membrane fabrication, GO membranes were also prepared on cellulose nitrate (CN) with 200-nm pores (Whatman). Free-standing GO film with a thickness ~10 μm was fabricated by applying the same vacuum filtration process, however, on porous anodic aluminum oxide (AAO) with 20-nm pores (Whatman). After drying overnight, the GO film can be easily peeled off, forming a free-standing GO film. Ultrathin GO membranes, such as 10-nm GO membrane on AAO as reported in ref. 19, was also fabricated for the comparison of membrane performance.

Hexadecane (HD) and octane serving as oil pollutants were purchased from Sigma-Aldrich. HD-in-water or octane-in-water emulsion were prepared by dissolving

100 mg of sodium dodecyl sulfate (SDS) in 1 L of DI water, and then mixed with 1.5 g of HD or octane, followed by 1 hour sonication to form an oil-in-water emulsion. The excellent stability of the emulsions was observed visually over at least 24-h period.

A self-designed stainless steel dead-end module with an active permeation area of 5.06 cm^2 was used for the water/oil separation experiments, as shown in Figure 3.5A. The feed side was connected to a high pressure nitrogen tank, which provided a driving force of 1 bar for pure water permeation and water/oil separation experiments. An electronic scale (Ohaus, CS Series) was used to measure the filtrate mass. Before oil emulsion separation test, 1-hour pure water permeation was firstly conducted to get the initial pure water flux. The oil-in-water emulsion was then poured into the module with water pre-wetted membranes. Oil emulsion separation test was conducted for 2 h, during which we took 2 samples of the filtrate (1 mL each) at 1 h and 2 h, respectively, for later oil rejection measurements. Afterwards, a simple membrane cleaning process was conducted by carefully flushing the membrane surface with tap water. The pure water permeation, oil emulsion separation, and the cleaning process together were considered as a single membrane performance evaluation cycle. The cycle was repeated for 3 to 5 times to systematically investigate the membrane fouling behavior and their recovery capability.

3.4.1 Characterizations

X-ray diffraction (XRD) study of GO membranes

XRD was carried out using a Rigaku MiniFlex II diffractometer with Cu Kα radiation ($\lambda = 0.15418$ nm) on free-standing GO films (~10 μm in thickness). A 3M double-sided tap was used as the substrate which was tested to have minimum background as well as few interfering peaks in required 2θ range. The XRD patterns data

were collected at 2θ angles in the range of 5 °to 35 °. Scherrer equations is applied to calculate the d-spacing of the characteristic diffraction peak (002) of GO.

X-ray photoelectron spectroscopy (XPS) analysis of GO membranes

The surface chemical compositions of the GO film (~10 μm in thickness) were analyzed by XPS (Kratos Axis Ultra DLD instrument equipped with a monochromated Al Ka x-ray source and hemispherical analyzer capable of an energy resolution of 0.5 eV). The peaks of the XPS binding energies were deconvoluted with Gaussian peak shapes using Origin package software.

Atomic force microscopy (AFM) study of GO flakes and membranes

To prepare samples for AFM imaging, 0.001 mg/mL GO suspensions were first diluted 500 times. 5 μL diluted suspension was deposited onto freshly cleaved mica dishes (Ted Pella, Inc.) and dried overnight at room temperature (about 298K). The deposited GO sheets were imaged using tapping-mode AFM of a Multimode Nanoscope V system (Veeco (now Bruker), Santa Barbara, CA). The measurements were performed using commercial Si cantilevers with a nominal spring constant and resonance frequency at 20-80 N/m and 230-410 kHz, respectively (TESP, Bruker AFM Probes, Santa Barbara, CA). The height and phase images were acquired simultaneously at the set-point ratio A/A_o = 0.9-0.95, where A and A_o refer to the "tapping" and "free" cantilever amplitudes, respectively. The AFM topography images were analyzed using image analysis software (Nanoscope III, Version 5.30r3.sr3, 2005). It was observed that GO sheet is a typical single-layer GO flake with a dimension of about ~ 1 μm. The height profile diagram (Figure 3.3B) of the AFM image showed that the thickness of the single-layer GO sheet was about 0.9 nm, which is consistent with the typical thickness of the observed SLGO[19].

Field emission scanning electron microscopy (FE-SEM) study of GO membranes

The FE-SEM (Zeiss Ultraplus Thermal Field Emission Scanning Electron Microscope) images in low and high magnifications were captured on the surfaces of porous supports and GO membranes. All the samples were uncoated so as to give a detailed visualization of local surface architectures. A low voltage between 2~5 kV, a low working distance < 4 mm, and a smaller capture size < 20 mm were applied to get satisfactory images.

Contact angle (CA) measurements and drag force tests

Videos of water/HD contact angle in air measurements were taken using VCP optima system (Model: Optima XE). Water/HD droplets (1~2 μL) were dropped carefully onto the surfaces of GO membranes as well as PA supports. Water/HD wetting behaviors were recorded from the beginning to the time when a 0 °contact angle was observed. Still images were obtained by snapshot of videos at the exact time points.

Underwater HD contact angle measurements were conducted with a self-designed system including a clear quartz cell serving as the water reservoir and a hooked microsyringe needle. Before the measurements, all samples were first wetted by water and then fixed reversely inside quartz cell which was filled with water. The hooked needle was then moved underneath the membrane sample. Similar volume of HD (1~1.5 μL) was delivered by microsyringe to the hooked needle tip. The base with quartz cell on top was then gently lowered to the point where the sample surface was just in contact with oil droplet. After that, the base was slowly resumed to a safe position. In the meantime, membrane/support started to drag the HD droplet until 'detached'. The whole process was videotaped. For surfaces with high oil adhesive force (such as PA), the oil

droplet was eventually displaced from the needle top and adhered to the surface. However, for surfaces with thin GO coatings, such as 10 nm, very weak oil adhesion was observed, as the oil droplet cannot be pulled away by contacting with the GO surface. To release the oil droplet from the needle, repeated fiddling of the needle tip were performed using lab tweezers. After that, the HD droplet floated upwards and then came in contact with the GO membrane surface, forming an oil/water/solid interface. A series of underwater HD contact angles were measured on the bare PA support and the GO membranes with different thickness (> 5 locations for each membrane or support). The simulated drag force tests had the similar operation procedures to that of video underwater HD contact angle measuremen.

Total organic carbon (TOC) analysis for oil rejection measurement

Oil rejection was measured using total organic carbon (TOC) analysis method. For each tested membrane or support, we took two filtrate samples during 2 hours emulsion separation tests of each cycle, at 1 hour and 2 hour, respectively. After separation tests, filtrate samples were firstly diluted by 20 times, and then acidified below a pH of 2.0 by adding 10 wt% sulfuric acid to prevent the loss of compounds for dissolved organic carbon analysis. Analysis of organic compounds in these samples was performed using a TOC analyzer (TOC-V_{CSN}, Shimadzu Scientific Instruments, Columbia, MD, USA). Since the total organic carbon in the feed emulsion was known, the organic rejection ratio could therefore be calculated as Oil Rejection = $[1 - (TOC_{filtrate}/TOC_{feed})] \times 100\%$.

3.5 Conclusion

In conclusion, we have prepared novel GO membranes/coatings with hierarchical roughness to mimic the function and structure of fish scales. Our results clearly showed the superior anti-fouling performance of this new class of GO membranes/coatings. We anticipate this concept is generic, and can be applied to plenty of other commercially available porous supports with rough surfaces, and thus may generate a group of low-adhesion, underwater superoleophobic membranes/materials for wide applications in oil-polluted water.

3.6 Acknowledgements

We acknowledge support from USC start-up funding and experimental assistance on XPS and contact angle measurements by Shuguo Ma and Sheng Feng, respectively.

3.7 References

[1] L. Feng, Z. Zhang, Z. Mai, Y. Ma, B. Liu, L. Jiang, D. Zhu, *Angewandte Chemie* **2004**, *116*, 2046.

[2] M. Nosonovsky, P. K. Rohatgi, *Biomimetics in Materials Science Self-Healing, Self-Lubricating, and Self-Cleaning Materials*, Springer-Verlag, New York **2012**.

[3] C. H. Peterson, S. D. Rice, J. W. Short, D. Esler, J. L. Bodkin, B. E. Ballachey, D. B. Irons, *Science* **2003**, *302*, 2082.

[4] J. K. Yuan, X. G. Liu, O. Akbulut, J. Q. Hu, S. L. Suib, J. Kong, F. Stellacci, *Nature Nanotechnology* **2008**, *3*, 332.

[5] A. Tuteja, W. Choi, M. L. Ma, J. M. Mabry, S. A. Mazzella, G. C. Rutledge, G. H. McKinley, R. E. Cohen, *Science* **2007**, *318*, 1618.

[6] L. Lin, M. J. Liu, L. Chen, P. P. Chen, J. Ma, D. Han, L. Jiang, *Advanced Materials* **2010**, *22*, 4826.

[7] K. S. Liu, Y. Tian, L. Jiang, *Progress in Materials Science* **2013**, *58*, 503.

[8] M. J. Liu, S. T. Wang, Z. X. Wei, Y. L. Song, L. Jiang, *Advanced Materials* **2009**, *21*, 665.

[9] P. C. Chen, Z. K. Xu, *Scientific Reports* **2013**, *3*, 6.

[10] A. K. Kota, G. Kwon, W. Choi, J. M. Mabry, A. Tuteja, *Nature Communications* **2012**, *3*, 8.

[11] G. Kwon, A. K. Kota, Y. X. Li, A. Sohani, J. M. Mabry, A. Tuteja, *Advanced Materials* **2012**, *24*, 3666.

[12] Q. Wen, J. C. Di, L. Jiang, J. H. Yu, R. R. Xu, *Chemical Science* **2013**, *4*, 591.

[13] Z. X. Xue, S. T. Wang, L. Lin, L. Chen, M. J. Liu, L. Feng, L. Jiang, *Advanced Materials* **2011**, *23*, 4270.

[14] D. A. Dikin, S. Stankovich, E. J. Zimney, R. D. Piner, G. H. B. Dommett, G. Evmenenko, S. T. Nguyen, R. S. Ruoff, *Nature* **2007**, *448*, 457.

[15] C. Lee, X. D. Wei, J. W. Kysar, J. Hone, *Science* **2008**, *321*, 385.

[16] R. K. Joshi, P. Carbone, F. C. Wang, V. G. Kravets, Y. Su, I. V. Grigorieva, H. A. Wu, A. K. Geim, R. R. Nair, *Science* **2014**, *343*, 752.

[17] H. W. Kim, H. W. Yoon, S. M. Yoon, B. M. Yoo, B. K. Ahn, Y. H. Cho, H. J. Shin, H. Yang, U. Paik, S. Kwon, J. Y. Choi, H. B. Park, *Science* **2013**, *342*, 91.

[18] S. P. Koenig, L. D. Wang, J. Pellegrino, J. S. Bunch, *Nature Nanotechnology* **2012**, *7*, 728.

[19] H. Li, Z. N. Song, X. J. Zhang, Y. Huang, S. G. Li, Y. T. Mao, H. J. Ploehn, Y. Bao, M. Yu, *Science* **2013**, *342*, 95.

[20] B. X. Mi, *Science* **2014**, *343*, 740.

[21] R. R. Nair, H. A. Wu, P. N. Jayaram, I. V. Grigorieva, A. K. Geim, *Science* **2012**, *335*, 442.

[22] J. Kim, L. J. Cote, F. Kim, W. Yuan, K. R. Shull, J. X. Huang, *Journal of the American Chemical Society* **2010**, *132*, 8180.

[23] J. A. Howarter, J. P. Youngblood, *Journal of Colloid and Interface Science* **2009**, *329*, 127.

[24] W. J. Chen, J. M. Peng, Y. L. Su, L. L. Zheng, L. J. Wang, Z. Y. Jiang, *Separation and Purification Technology* **2009**, *66*, 591.

[25] D. J. Miller, S. Kasemset, D. R. Paul, B. D. Freeman, *Journal of Membrane Science* **2014**, *454*, 505.

[26] H. H. Li, Y. M. Cao, H. J. Qin, X. M. Jie, T. H. Wang, J. H. Liu, Q. Yuan, *Journal of Membrane Science* **2006**, *279*, 328.

[27] A. Asatekin, A. M. Mayes, *Environmental Science & Technology* **2009**, *43*, 4487.

[28] W. J. Chen, Y. L. Su, L. L. Zheng, L. J. Wang, Z. Y. Jiang, *Journal of Membrane Science* **2009**, *337*, 98.

[29] J. E. Zhou, Q. B. Chang, Y. Q. Wang, J. M. Wang, G. Y. Meng, *Separation and Purification Technology* **2010**, *75*, 243.

[30] C. Yang, G. S. Zhang, N. P. Xu, J. Shi, *Journal of Membrane Science* **1998**, *142*, 235.

[31] Y. Sun, Y. Bai, J. Gu, C. Zhang, *Desalination and Water Treatment* **2013**, 1.

[32] R. Rozada, J. I. Paredes, S. Villar-Rodil, A. Martinez-Alonso, J. M. D. Tascon, Nano Research **2013**, 6, 216.

[33] R. W. Baker, Membrane Technology and Applications, Wiley, Weinheim **2004**

CHAPTER 4 TUNING UNDERWATER OLEOPHOBICITY OF GRAPHENE OXIDE COATINGS VIA UV IRRADIATION

4.1 Abstract

Ultraviolet (UV) was utilized to gradually modify the chemistry and structure of graphene oxide (GO) flakes, as confirmed by XPS and AFM. Ultrathin GO coatings/membranes, made from UV-irradiated flakes, showed tunable underwater oleophobicity. UV-treated, superoleophobic GO membrane exhibited excellent antifouling capability for oil/water separation

4.2 Introduction

Surfaces with controllable underwater oil-adhesion have attracted great attention due to their potential applications in oil/water separation, oil-repellent materials, microfluidic devices, anti-bioadhesion materials, and robust antifouling materials.[1-4] Fish scales are well known to own the underwater superoleophoic/low oil adhesive properties. Studies on fish scales have shown hydrophilic mucus layer and micro/nanoscaled surface roughness are essential for their superior performance.[5] Consistently, underwater oil wettability on a solid surface has been found to depend strongly on the surface chemical composition and roughness.[6,7] Graphene oxide (GO) is a well-known hydrophilic material due to its unique chemistry.[8] Oxygen-containing functional groups, such as carboxyl,

carbonyl, hydroxyl and epoxy, are distributed at edges and structural defects of GO flakes. Therefore, GO flakes with fine-tuned chemistry and roughness are promising material for fabricating surfaces with desired underwater oleophobicity.

Oxidative etching has been proven as an effective way to create or enlarge structural defects on graphene-based materials.[9, 10] Generated defects increased the nano-scaled roughness on the single GO flakes.[11] In addition, oxidative etching also improved the hydrophilicity of GO, probably resulting from the introduced oxygen groups around the expanded and/or newly-generated defects.[8, 12] Oxidative etching, therefore, seems a viable way of controlling underwater oleophobicity of GO by modifying GO morphology and hydrophilicity. However, precise control of the hydrophilicity/underwater oleophobicity of GO via oxidative etching has not been reported. One potential reason could be that etching reaction is in oxidative gas phase, which usually proceeds fast and is difficult to control.[9, 10] Also, only single or few-layered graphene-based suspended flakes or coatings, instead of powder, have been etched uniformly in gas phase,[9, 11] which may limit their large-scale productivity for potential applications. Here, we report the novel use of ultraviolet (UV) light to controllably modify the chemistry and structure of GO flakes in aqueous media. We demonstrate that by simply controlling the UV etching time for dispersed GO flakes in water, the resulting GO coatings can be converted into underwater superoleophobic coatings. In addition, this method is very promising for large-scale production. Cyclic oil/water separation tests of the UV-treated, superoleophobic GO coatings/membranes exhibited excellent antifouling and ease-of-cleaning performance. Such an effective and facile methodology to modify the chemistry

and morphology of GO flakes may provide great opportunities to generate functional coatings/surfaces with drastically improved underwater oil repellence.

4.3 Experimental Results and Discussion

We prepared GO by an improved Hummers' method.[13] Dry GO powder was then well dispersed in deionized (DI) water by ultrasonication. After centrifugation, GO agglomerates were removed. The final GO flakes are ~1000 nm in size (Figure 4.1A) and single-layered (Figure 4.1B), as confirmed by atomic force microscopy (AFM). We then diluted the GO dispersion to a concentration of 0.0625 mg/mL. A UV lamp was applied as the light source to conduct etching treatment of the GO dispersion for different times, from 0 to 90 min (labelled as 0-GO, 10-GO, 30-GO, 60-GO and 90-GO for convenience). UV treatment in water, instead of in air, provides us better control of the GO etching process. This is because good dispersion of GO in water and vigorous stir ensure uniform UV irradiation for GO flakes. The GO dispersion was then used to fabricate 10-nm coatings/membranes onto flat anodic aluminium oxide (AAO) supports (20-nm pore size) by a vacuum filtration method, following a similar procedure from our previous work.[14] Water contact angle in air and oil contact angle in water measurements were subsequently performed for the GO coatings/membranes (see Supporting Information for experimental details). As shown in Figure 4.1C, the water contact angle in air decreases gradually with the increase of UV treatment time, from 70.0 ° for 0-GO membrane to 32.4 ° for 90-GO membrane. From the underwater hexadecane (HD) contact angle measurements, slight contact angle increase from 0-GO to 30-GO could be noticed. Surprisingly, we found that when UV treatment time increased to 60 min, the underwater oil contact angle became 159.1 °, which is considered to be superoleophobic (>150^{o}).[15] The 90-GO membrane

shows even higher oil contact angle (167.2 ◦) than the 60-GO membrane. These results indicate that the oil-adhesion characteristics in oil-water-solid triple-phase system could be tuned by changing UV exposure time (see Supporting Information for details).

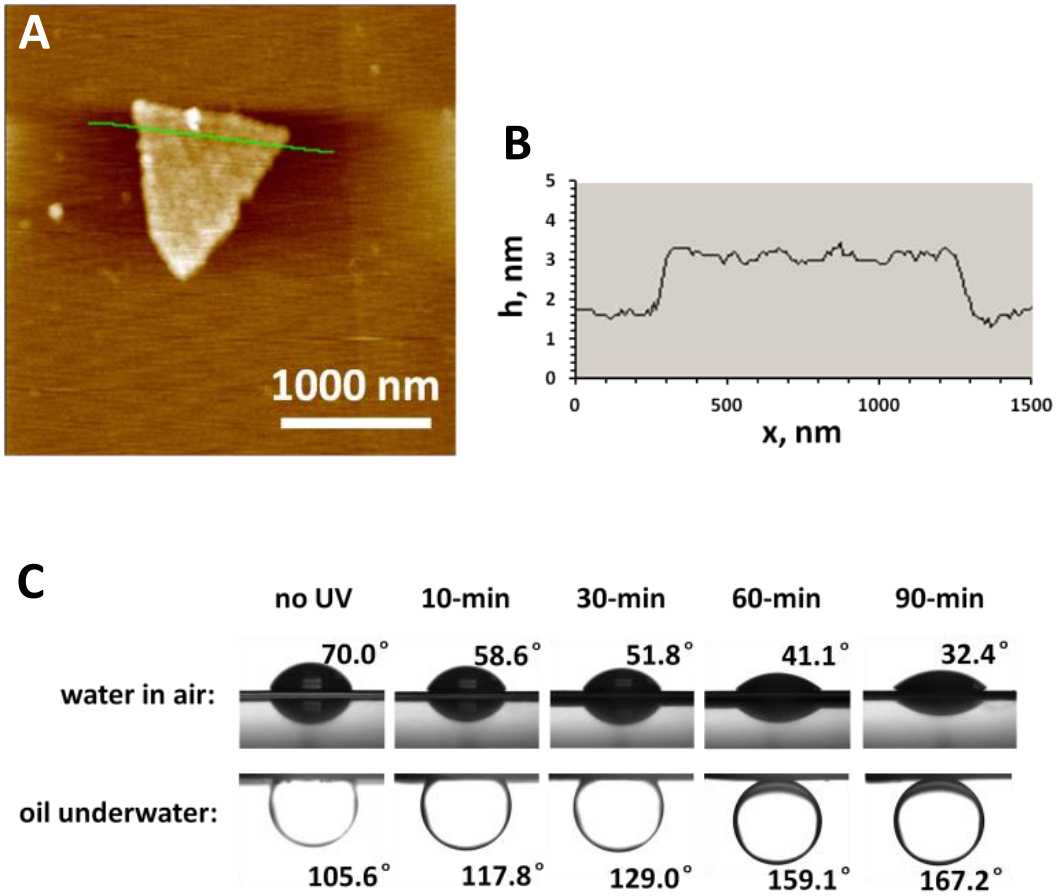

Figure 4. 1 (A) AFM image of a GO flake on a freshly cleaved mica. (B) The height profile across the green line in (A). h, height; x, position. (C) Water contact angle in air and hexadecane (HD) contact angle in water for GO membranes with different UV treatment times.

To explain the underlying mechanism, we further conducted x-ray photoelectron spectroscopy (XPS) and Raman spectroscopy measurements for GO dispersion after different UV treatment times. After deconvoluting the overlapping XPS peaks of C_1s (see Figure 4.2 for C_1s XPS spectra), percentage of carbon in different chemical environments can be obtained, as shown in Figure 4.3A. It is seen that as the UV treatment time increased, the percentage of oxidized carbon (including C-O, C=O and COOH) increased. This is because percentage of C in C=O and COOH increased, whereas that of C-O didn't change much. These groups on GO have been proved to have strong affinity to water molecules,[16] and thus would help form a thin layer of water barrier to lower the oil adhesion. Higher percentage of hydrophilic oxygen-containing functional groups after longer UV treatment time, therefore, may contribute to the better wettability of water in air and lower oil-adhesion underwater. Raman spectra (Figure 4.3B) show that the I_D/I_G ratio increased as the UV treatment time increased, suggesting higher disorder of the planar structure of the GO flakes. This may be caused by the enlarged or newly-generated structural defects.[9] We then deposited thin coatings onto mica using GO dispersions with different UV exposure times and directly conducted AFM on them, as shown in Figure 4.4A to D. We can see that for the 0-GO coating, the surface is fairly flat and continuous. The 30-GO coating shows a surface decorated with defects from ~80 to 120 nm in size, while the 60-GO coating exhibits a very disordered surface with large holes from ~300 to 500 nm. The 90-GO coating seems more like isolated islands, apparently due to the over-etching.[10, 11] The generated defects eventually increased the nano-scaled surface roughness of the GO coatings, as indicated by the height profiles. Therefore, we conclude that both the chemical composition and structure

changes after UV oxidative etching lead to the drastically improved underwater oleophobicity of GO coatings (see Supporting Information for details).

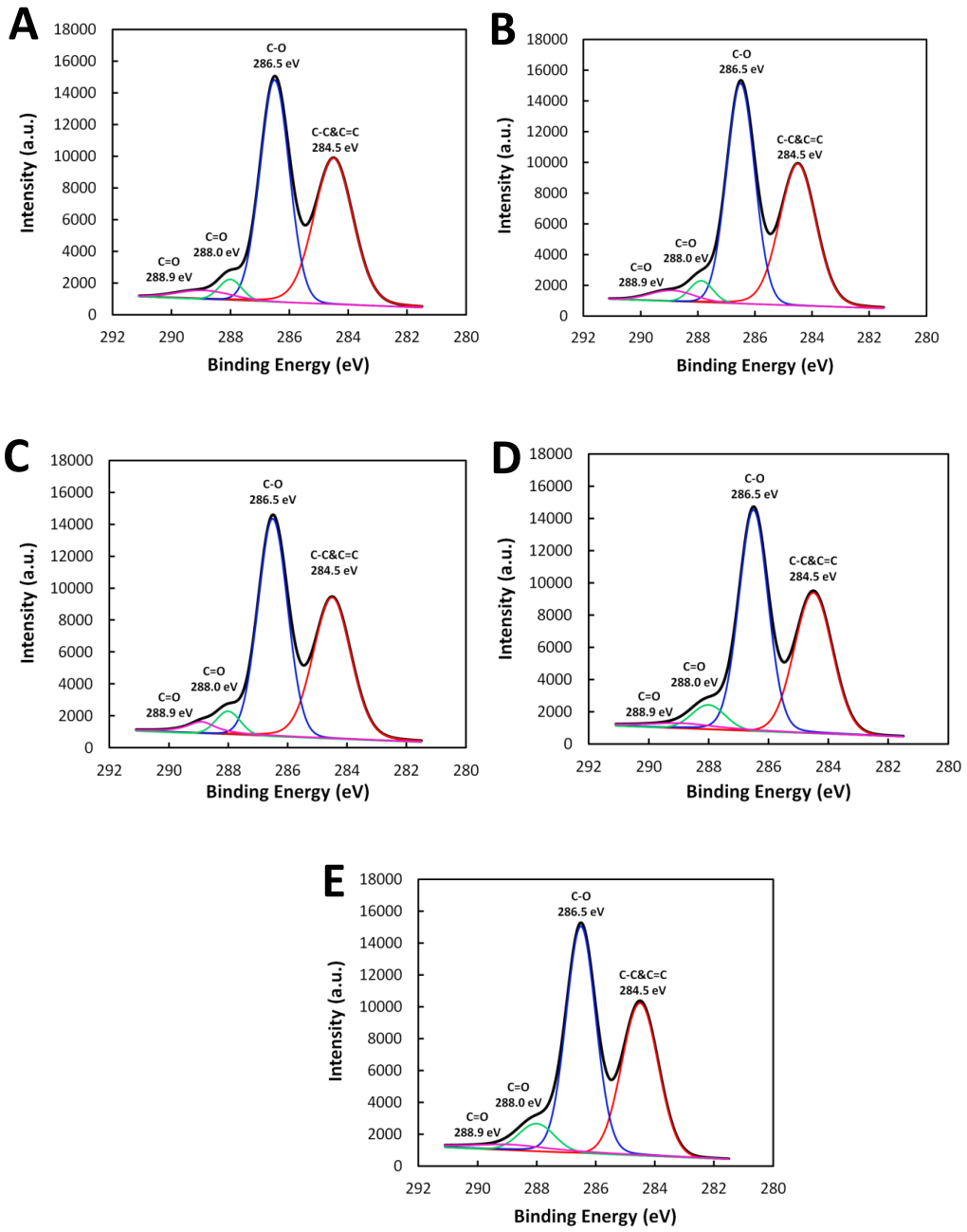

Figure 4. 2 XPS C_1s spectra for (A) 0-GO, (B) 10-GO, (C) 30-GO, (D) 60-GO and (E) 90-GO.

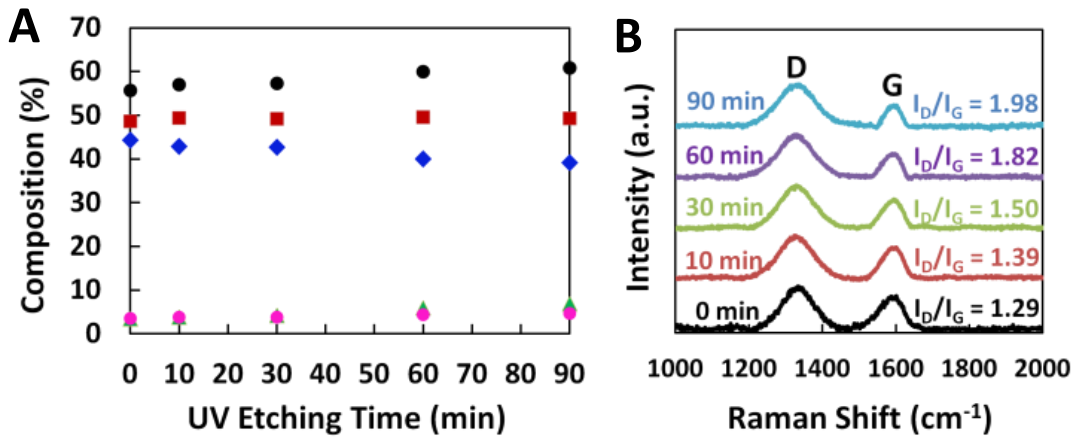

Figure 4. 3 (A) Percentage of differently bonded carbon on GO analyzed by XPS: ● Total oxidized carbon; ◆ Total unoxidized carbon; ■ C-O; ▲ C=O; ● COOH; (B) Raman spectra of GO after different UV treatment times from 0 to 90 min.

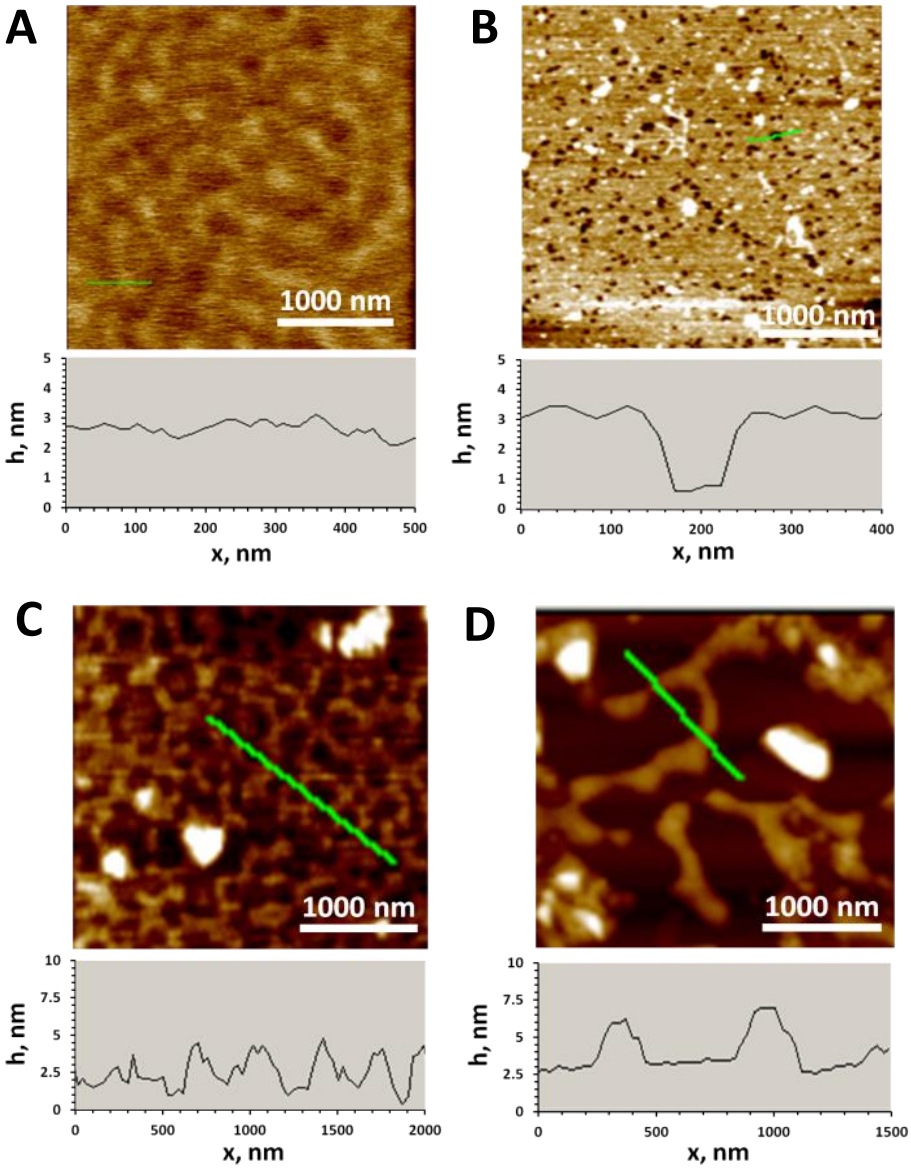

Figure 4. 4 AFM images and height profiles across the green lines for (A) 0-GO coating, (B) 30-GO coating, (C) 60-GO coating, and (D) 90-GO coating on mica. h, height; x, position

As is known, fouling of nano/ultrafiltration membranes in oil/water separation is a longstanding issue and a major economic barrier for their wide application.[17] Membranes with underwater superoleophobic surfaces are of great potential to realize antifouling in the oily wastewater treatment.[18] In order to utilize such excellent underwater superoleophobicity of our UV-treated GO, we prepared 10-nm GO membranes on polyamide (PA) supports using UV-treated GO (0, 30 and 60-GO) and conducted a series of oil emulsion filtration in a dead-end system to investigate their antifouling performance. 1500 ppm HD-in-water emulsion, stabilized by 100 ppm sodium dodecyl sulfate (SDS) after 1 hour sonication, was used as feed. The filtration process contains three cycles. In each individual cycle, a pure water filtration was performed, followed by an emulsion separation. During the interval between two neighboring cycles, a simple water flush cleaning process was applied to clean the membrane surface. Therefore, the recovery of pure water flux in each cycle could be an indicator of the membrane fouling degree. 60-GO membrane shows ~100% pure water recovery for all cycles (Figure 4.5), suggesting superior antifouling performance. In stark contrast, 0-GO membrane (Figure 4.6A) exhibits severe membrane fouling, since the pure water flux recovery for the 2nd cycle is only 51.7% and further decreases for the 3rd cycle. 30-GO membrane (Figure 4.6B) shows improved antifouling performance with 2nd cycle pure water flux recovery of 90.1%. This again validates our methodology of utilizing UV to tune the chemical composition and structure of GO flakes to realize low oil-adhesion, underwater superoleophobic surface. The oil rejection for the tested membranes was all around 98.0%, (see Supporting Information for detailed experimental setup and discussion).

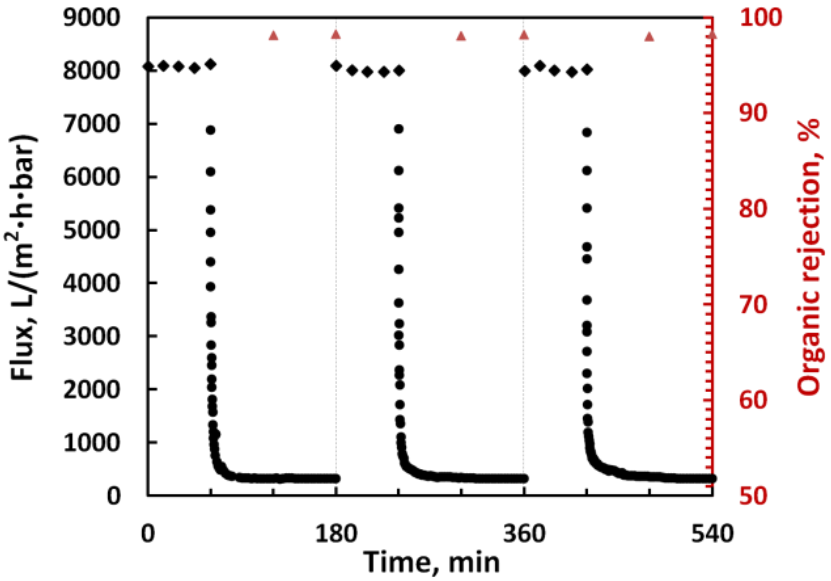

Figure 4. 5 Cyclic water/oil separation test for a 10-nm 60-GO membrane on PA support. (●) total flux in oil-in-water emulsion separation. (◆) pure water flux. (▲) total organic rejection,

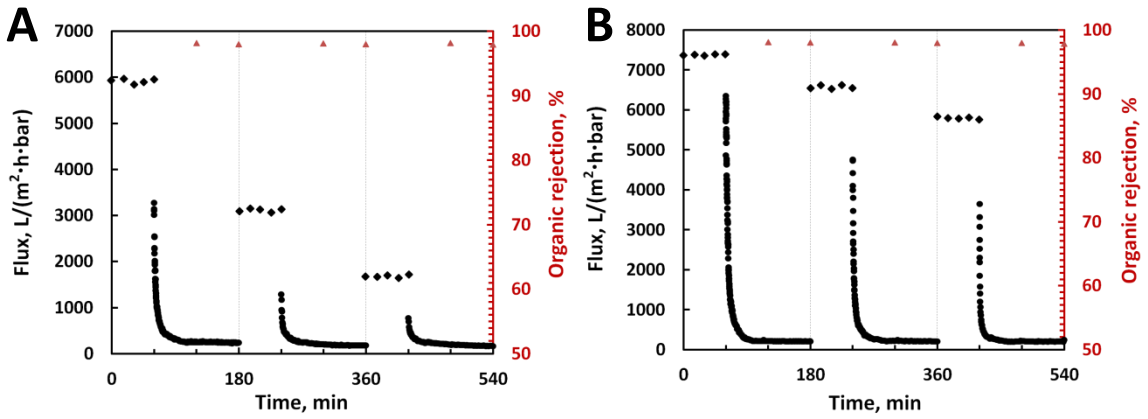

Figure 4. 6 Cyclic water/oil separation tests for (A) 10-nm 0-GO membrane and (B) 10-nm 10-GO membrane. (●) total flux in oil-in-water emulsion separation. (◆) pure water flux. (▲) total organic rejection.

4.4 Supporting Information

4.4.1 Materials and Methods

We synthesized graphene oxide (GO) powder by an improved Hummers' method.[13] Concentrated H_2SO_4 (69 mL) was slowly added into the mixture of graphite flakes (3.0 g) and $NaNO_3$ (1.5 g). The mixture was cooled down to 0 ^oC in a ice bath. $KMnO_4$ (9.0 g) was then added into the mixture slowly. The mixture was kept at 35 ^oC and stirred for 30 min. Subsequently, 138 mL water was slowly added into the mixture. This produced large amount of heat and raised the reaction temperature up to 98 ^oC. The mixture temperature stayed at 98 ^oC for 2 h and then slowly cooled down by water bath. Additional 420 mL water and 3 mL of H_2O_2 (30%) were added into the mixture. After cooling down to the room temperature, the product was collected by vacuum filtration. The final GO product was washed with 200 mL water, 200 mL 1 mol/L HCl, and 200 mL ethanol for two times. The as-prepared GO was dried in vacuum oven at 40 ^oC first and then made into 2 mg/mL GO dispersion by sonication in DI water for 1 hour. Centrifugation was performed for the GO dispersion at 10,000 rpm for 30 min to remove large agglomerations.

We used a UV lamp (B-100Y, Mineralogical Research Company) to treat the centrifuged GO dispersion with different time, 0, 10, 30, 60 and 90 min. In order to achieve the uniformity of the UV treatment, a magnetic stirrer was applied and kept rotating in the GO dispersion when UV etching was performed. The treated GO dispersions were labeled as 0-GO, 10-GO, 30-GO, 60-GO and 90-GO, where 0-GO means GO dispersion with 0 min UV treatment, and so on.

GO membranes were fabricated by a vacuum filtration method, as described in our previous study.[14] For contact angle measurements, we chose anodic aluminum oxide (AAO, 20-nm pore size, Whatman) as the filtration support. For water/oil separation tests, we selected polyamide (PA, 200-nm cut-off pore size, Whatman) as the filtration support. The membranes were dried under vacuum for 12 hours at room temperature. We then closed the vacuum and let it release naturally for good membrane quality.

4.4.2 Characterizations

Atomic force microscopy (AFM) study of GO flakes and coatings

We used atomic force microscope (AFM) to image both individual GO flakes and GO coatings. To prepare samples for individual GO flake imaging, 0.001 mg/mL GO suspensions (with UV treatment time from 0 to 90 min) were first diluted 500 times. A 4 uL drop of diluted suspension was deposited onto freshly cleaved muscovite mica disks (9.9 mm diameter, Grade V1, Structure Probe, Inc.). For continuous GO coatings imaging, 0.0625 mg/mL GO dispersions (with UV treatment time from 0 to 90 min) was first diluted 30 times and then dropped (1 drop) onto clean mica. Both types of samples were dried for 10 min at 40 ^{o}C prior to AFM imaging. The deposited GO flakes or coatings were imaged using a PicoPlus AFM (Agilent) operated in the tapping mode. All images were collected using N-type silicon cantilevers (FORTA-50, Nanoscience Instruments, Inc.) with spring constants of 1.2-6.4 N/m, resonance frequencies of 47-76 kHz, and nominal tip radius of < 10 nm. The height resolution of the AFM scanner is less than 1 A. Thus, with proper calibration, the accuracy of the measured height of surface features is approximately ±0.1 nm. The AFM topography images were analyzed using image

analysis software (Scanning Probe Image Processor or SPIP, Image Metrology A/S, Denmark).

Contact angle (CA) measurements

Water contact angle in air measurements were taken using VCP optima system (Model: Optima XE). Water droplets (1~2 μL) were dropped carefully onto the surfaces of GO membranes on AAO. Underwater HD contact angle measurements were conducted with a self-designed system including a clear quartz cell serving as the water reservoir and a hooked microsyringe needle. Before the measurements, all samples were first wetted by water and then fixed reversely inside quartz cell which was filled with water.

X-ray photoelectron spectroscopy (XPS) analysis

The surface chemical compositions of the GO were analyzed by XPS (Kratos Axis Ultra DLD instrument equipped with a monochromated Al Ka x-ray source and hemispherical analyzer capable of an energy resolution of 0.5 eV). To prepare samples for XPS analysis, we deposited 1 drop of 0.0625 mg/mL GO dispersion on to clean silicon wafer and dried at 40 ^{o}C. For C_1s, the signal was fitted by four components: C-C&C=C (284.5 eV), C-O (286.5 eV), C=O (288.0 eV) and O=C-OH (289.0 eV), as shown in Figure 4.2A to E, which are consistent with those have been reported.[19] By integration of each individual peak, the composition for each carbon species could be calculated.

Raman spectroscopy analysis

Raman spectroscopy was performed on LabRam HR confocal Raman spectrometer (JY Horiba). The spectrometer is equipped with a liquid-nitrogen cooled,

charge-coupled device (CCD) detector, and a He-Ne (632.817 nm) laser for excitation. For sample preparation, 1 drop of 0.0625 mg/mL GO dispersion was deposited on to a glass slide and dried at 40 ^{o}C for 20 min. The well-known Raman characteristics of carbon materials are the G and D bands (1580 and 1350 cm^{-1}) which are usually assigned to the graphitized structure and local defects/disorders particularly located at the edges of graphene and graphite platelets, respectively.[20, 21] Therefore, a larger I_D/I_G peak intensity ratio can be assigned to higher defects/disorders in the graphitized structure.

Total organic carbon (TOC) analysis

Oil rejection was measured using total organic carbon (TOC) analysis method. For each tested membrane or support, we took two filtrate samples during 2 hours emulsion separation tests of each cycle, at 1 hour and 2 hour, respectively. After separation tests, filtrate samples were firstly diluted by 20 times, and then acidified below a pH of 2.0 by adding 10 wt% sulfuric acid to prevent the loss of compounds for dissolved organic carbon analysis. Analysis of organic compounds in these samples was performed using a TOC analyzer (TOC-V_{CSN}, Shimadzu Scientific Instruments, Columbia, MD, USA). Since the total organic carbon in the feed emulsion was known, the organic rejection ratio could therefore be calculated as Oil Rejection = [1 – ($TOC_{filtrate}/TOC_{feed}$)] ×100%.

4.4.3 Filtration System Setup

A self-designed stainless steel dead-end module with an effective permeation area of 5.06 cm^2 was used for the water/oil separation experiments. The feed side was connected to a high pressure nitrogen tank, which provided a driving force of 1 bar for

pure water permeation and water/oil separation experiments. A magnetic stirring bar was used above the membrane (module placed on a stir table), and kept rotating while permeation/separation tests were performed. An electronic scale (Ohaus, CS Series) was used to measure the filtrate mass. Before oil emulsion separation test, 1-hour pure water permeation was firstly conducted to get the initial pure water flux. The oil-in-water emulsion was then poured into the module with water pre-wetted membranes. Oil emulsion separation test was conducted for 2 h, during which we took 2 samples of the filtrate (1 mL each) at 1 h and 2 h, respectively, for later oil rejection measurements. Afterwards, a simple membrane cleaning process was conducted by carefully flushing the membrane surface with tap water. The pure water permeation, oil emulsion separation, and the cleaning process together were considered as a single membrane performance evaluation cycle. The cycle was repeated 3 times to systematically investigate the membrane fouling behavior and their recovery capability. The filtration process contains three cycles. In each individual cycle, a pure water filtration was performed, followed by an emulsion separation. During the interval between two neighbouring cycles, a simple water flush cleaning process was applied to clean the membrane surface. Figure 4.6A shows the performance of a 10-nm 0-GO membrane. For the first cycle, pure water flux through the fresh 0-GO membrane was constant at ~5900 L/(m^2·h·bar) within 1 hour. The initial permeate flux during emulsion separation was 3275 L/(m^2·h·bar), and decreased down to 250 L/(m^2·h·bar) after two hours. For the second cycle, pure water flux could be recovered to about 52% of the one in the first cycle. The initial permeate flux in emulsion separation was recovered to 1290 L/(m^2·h·bar) and further decreased to 180 L/(m^2·h·bar). Similar trend was observed for the third cycle. The above results indicate that severe

membrane fouling occurred during the emulsion separation. We then tested the performance of a 10-nm 30-GO membrane, as shown in Figure 4.6B. Compared with 0-GO membrane, 30-GO membrane shows both higher pure water flux (~7400 $L/(m^2 \cdot h \cdot bar)$) and initial permeate flux (~6360 $L/(m^2 \cdot h \cdot bar)$) during the emulsion separation in the first cycle. Besides, the pure water recovery (89%) in the second cycle was much higher than that of 0-GO. Similar trend was found in the following cycles. Better antifouling performance of the 30-GO membrane could be attributed to the decreased oil adhesion on the surface, as indicated by the underwater oil contact angle results. Figure 4.5 exhibits the separation performance of the 60-GO membrane. It is noticed that for the first cycle, both the pure water flux and initial permeate flux during emulsion separation which was ~8100 and ~6870 $L/(m^2 \cdot h \cdot bar)$, respectively, are higher than those of 0-GO and 10-GO membranes, Also, these values could be maintained for the following two cycles.

4.5 Conclusions

In summary, UV-irradiation was utilized as an effective and facile approach to tune underwater oleophobicity of GO coatings/membranes by gradually modifying GO flake composition and surface morphology. Superoleophobic GO membranes, made from UV-treated GO flakes, showed excellent antifouling capability and greatly improved oil emulsion separation performance. We expect this facile strategy to tune underwater oleophobicity of GO may help design novel graphene-based materials/coatings for wide applications in oil contaminated environments.

4.6 Acknowledgement

We acknowledge the financial support from USC start-up funding and USC SPARC graduate student grant. We also thank Drs Shuguo Ma, Qian Wang and Xinyu Huang for their experimental assistance on XPS, contact angle and Raman, respectively.

4.7 References

1. A. K. Geim, S. V. Dubonos, I. V. Grigorieva, K. S. Novoselov, A. A. Zhukov and S. Y. Shapoval, *Nat Mater*, 2003, **2**, 461-463.

2. Y. Huang, M. Liu, J. Wang, J. Zhou, L. Wang, Y. Song and L. Jiang, *Advanced Functional Materials*, **21**, 4436-4441.

3. D. Tian, Z. Guo, Y. Wang, W. Li, X. Zhang, J. Zhai and L. Jiang, *Advanced Functional Materials*, **24**, 536-542.

4. M. Liu, X. Liu, C. Ding, Z. Wei, Y. Zhu and L. Jiang, *Soft Matter*, **7**, 4163-4165.

5. K. Liu, Y. Tian and L. Jiang, *Progress in Materials Science*, **58**, 503-564.

6. T. Sun, G. Qing, B. Su and L. Jiang, *Chemical Society Reviews*, **40**, 2909-2921.

7. R. Blossey, *Nat Mater*, 2003, **2**, 301-306.

8. D. R. Dreyer, S. Park, C. W. Bielawski and R. S. Ruoff, *Chemical Society Reviews*, **39**, 228-240.

9. S. P. Koenig, L. Wang, J. Pellegrino and J. S. Bunch, *Nat Nano*, **7**, 728-732.

10. Z. Zeng, X. Huang, Z. Yin, H. Li, Y. Chen, H. Li, Q. Zhang, J. Ma, F. Boey and H. Zhang, *Advanced Materials*, **24**, 4138-4142.

11. T. H. Han, Y.-K. Huang, A. T. L. Tan, V. P. Dravid and J. Huang, *Journal of the American Chemical Society*, **133**, 15264-15267.

12. A. Bagri, C. Mattevi, M. Acik, Y. J. Chabal, M. Chhowalla and V. B. Shenoy, *Nat Chem*, **2**, 581-587.

13. D. C. Marcano, D. V. Kosynkin, J. M. Berlin, A. Sinitskii, Z. Sun, A. Slesarev, L. B. Alemany, W. Lu and J. M. Tour, *ACS Nano*, **4**, 4806-4814.

14. H. Li, Z. Song, X. Zhang, Y. Huang, S. Li, Y. Mao, H. J. Ploehn, Y. Bao and M. Yu, *Science*, **342**, 95-98.

15. A. K. Kota, G. Kwon, W. Choi, J. M. Mabry and A. Tuteja, *Nat Commun*, **3**, 1025.

16. R. R. Nair, H. A. Wu, P. N. Jayaram, I. V. Grigorieva and A. K. Geim, *Science*, **335**, 442-444.

17. A. Asatekin and A. M. Mayes, *Environmental Science & Technology*, 2009, **43**, 4487-4492.

18. L. Zhang, Z. Zhang and P. Wang, *NPG Asia Mater*, **4**, e8.

19. J. Shang, L. Ma, J. Li, W. Ai, T. Yu and G. G. Gurzadyan, *Sci. Rep.*, **2**.

20. A. C. Ferrari and J. Robertson, *Physical Review B*, 2000, **61**, 14095-14107.

21. D. Graf, F. Molitor, K. Ensslin, C. Stampfer, A. Jungen, C. Hierold and L. Wirtz, *Nano Letters*, 2007, **7**, 238-242.

CHAPTER 5 CONCLUSIONS

This study mainly focus on the GO membrane and its application for membrane separations. By a variety of characterizations, both the structural and chemical properties of GO were systematically investigated. To utilize these unique properties of GO, GO membranes were successfully fabricated for both H_2 separations, as well as oil/water separations. Fundamental separation mechanisms were studied, including molecular sieving for H_2 separations and underwater oleophobicity/low oil-adhesion for oil/water separation. Finally, a facile method to tune the GO chemistry and structure was demonstrated, which indicated the potential of graphene-based materials in modification for improved membrane separation performance.

First, ultrathin GO membranes with thickness down to 1.8 nm, were prepared on AAO supports, which represented the thinnest membrane in the world. It is proved that due to the strong oxidative environment of GO synthesis, structural defects existed on GO flakes. After single and mixture gas separation tests, ultrathin GO membranes showed both high H_2/CO_2 and H_2/N_2 selectivities, which were 3400 and 700, respectively, while maintaining a relatively high H_2 permeance. The superior H_2 separation performance of GO membranes was above Robeson upper bound. This can be attributed to the molecular sieving of selective structural defects in GO that act as the H_2 transport pathway and block larger gas molecules.

The application was further extended to oil/water separation of the GO membranes. Flat GO membranes showed amphiphilic in air and oleophobic under water. However, after introduction of a hierarchical roughness by the combination of GO self-corrugation and the intrinsic roughness provided by the underneath PA support, the underwater oleophobicity of GO membranes could be improved to underwater superoleophobicity, indicating both the surface chemistry and morphology contributed to the underwater oil adhesion on GO membrane surface. Cyclic oil/water separation tests demonstrated that GO membranes with optimized hierarchical surface roughness possessed excellent antifouling performance and self-cleaning capability, while kept high filtrate flux. Compared with other reported ultrafiltration membranes, GO membranes showed superior performance with regarding to the filtrate flux and antifouling behavior.

At last, the feasibility of utilizing UV to uniformly etch GO to controllably tune the chemistry and morphology of GO flakes in aqueous media was demonstrated. Various characterizations, such as XPS and AFM, proved that after UV oxidative treatment, both the chemistry and structure of GO flakes were altered, due to the extra-induced hydrophilic groups and structural defects. Contact angle measurements revealed that the underwater oleophobicity of GO could be tuned by UV treatment time. Cyclic oil/water separation tests showed that the antifouling property of GO membranes could be improved by the UV oxidative etching method.